Chapter 3
The Two-Dimensional Case

3.1 General Notions

We now turn to the examination of the two-dimensional DNLS equation, and of the type of excitations that can emerge in that context.

The dynamical equation can be written in the form

$$i\dot{u}_{n,m} + \epsilon\left(u_{n+1,m} + u_{n-1,m} + u_{n,m+1} + u_{n,m-1} - 4u_{n,m}\right) + |u_{n,m}|^2 u_{n,m} = 0, \quad (3.1)$$

where $u_{n,m}$ represents the two-dimensional complex field. The corresponding Hamiltonian function of this Hamiltonian system can be expressed as

$$H = \sum_{(n,m)\in\mathbb{Z}^2} \epsilon|u_{n+1,m} - u_{n,m}|^2 + \epsilon|u_{n,m+1} - u_{n,m}|^2 - \frac{1}{2}|u_{n,m}|^4. \quad (3.2)$$

In addition to the time translational invariance inducing the conservation of the Hamiltonian, this infinite dimensional dynamical system also has the U(1) invariance, analogously to its one-dimensional sibling, hence it also preserves the squared l^2 norm or power $P = \sum_{m,n} |u_{n,m}|^2$. These are the two fundamental conservation laws that are known for the discrete case. In the continuum analog of the model, there exist additional conservation laws; a natural one among these corresponds to the vector form of the momentum

$$M = i\int \left(u\nabla u^\star - u^\star \nabla u\right) dxdy. \quad (3.3)$$

A far less obvious invariance of the two-dimensional setting is the so-called pseudo-conformal invariance which is *particular* to the two-dimensional case (the so-called critical case for the cubic nonlinearity). If one defines $l(t) = (t_\star - t)/t_0$, then the transformation $\mathbf{x}'(t) = \mathbf{x}(t)/l(t)$, $t' = \int_0^t ds/l^2(s)$ and $u'(\mathbf{x}', t') = lu(\mathbf{x}, t)\exp(ia|\mathbf{x}|^2/(4l^2))$, leaves the equation unchanged. In the above expressions, $a = -ldl/dt$ and $\mathbf{x}$ is used to denote the spatial vector. The corresponding conserved quantity is

P.G. Kevrekidis, *The Discrete Nonlinear Schrödinger Equation*, STMP 232, 55–98, DOI 10.1007/978-3-540-89199-4_3,

$$C = \int \left(|\mathbf{x}u + 2it\nabla u|^2 - 2t^2|u|^4 \right) d\mathbf{x}. \tag{3.4}$$

It is important to note that neither of these last two conservation laws is preserved in the discrete case. Furthermore, the continuum case is well known to lead to collapse in its dynamical evolution; see a detailed analysis of the relevant phenomena in [1].

In fact, the two-dimensional case is special as it is the "critical dimension" beyond which collapse is occurring. The pseudo-conformal invariance allows the rescaling of the amplitude and the width of the solution in a self-similar way, without costing energy and in this way gives rise to the possibility of the solution to collapse along this group orbit in finite time. In fact, if the power of the solution exceeds that of the fundamental, single-humped radial solution of the equation (often referred to as the Townes soliton [2]):

$$\Delta R + R - R^3 = 0, \tag{3.5}$$

then the initial condition leads to self-focusing and collapse, while if it is lower than that, it instead leads to dispersion. This collapse-type effect is of course no longer possible in the discrete case, since the l^2 conservation prevents any particular site from acquiring infinite amplitude (at best, the whole power of the initial condition may be concentrated on a single site, in a phenomenon referred to as *quasi-collapse*). Since the treatise of [1] addresses this issue in considerable detail (see also references therein), we will not discuss it further here. Instead we will focus on the stationary states of the discrete problem and their stability analysis.

As in the previous chapter, we will start by briefly discussing the single-pulse case, and we will then turn to more complex multisite solutions such as multipulse solitary waves and discrete vortices. The latter are a new feature of the two-dimensional discrete system with no direct analog in the one-dimensional infinite lattice case.

3.2 Single-Pulse Solitary Waves

The fundamental standing wave ($u_n = e^{i\Lambda t} v_n$) solution of the two-dimensional discrete equation should be a single-humped solitary wave that asymptotes to the Townes soliton [2] as the continuum limit is approached. Its stationary profile should satisfy

$$\Lambda v_n = \epsilon \Delta_2 v_n + v_n^3. \tag{3.6}$$

In view of the scaling property of the equation (under $\tilde{\Lambda} = \Lambda/\epsilon$ and the $\tilde{u}_n = u_n/\sqrt{\epsilon}$), ϵ (or Λ) can be scaled out, and we will consider the relevant problem of Eq. (3.6) monoparametrically.

In fact, we can consider this monoparametric problem at any dimension, if Δ_2 represents the corresponding d-dimensional discrete Laplacian (whereby site n has $2d$ neighbors). To obtain a semi-analytical understanding of the properties of the relevant ground state, we will analyze the problem of Eq. (2.65) starting with a variational approximation, which can be carried out at any dimension d. This approach for the single-pulse solutions of interest can be obtained using

$$v_n = Ae^{-a|n|_{l^1}}. \tag{3.7}$$

Then the Lagrangian from which Eq. (3.6) can be derived, namely

$$\mathcal{L}_{\text{eff}} = \sum_n \left(\sum_j 2\epsilon u_{n+e_j} u_n - (\Lambda + 2d\epsilon) u_n^2 + \frac{1}{2} u_n^4 \right), \tag{3.8}$$

(where e_j is the unit vector along the jth direction) can be explicitly evaluated as

$$\mathcal{L}_{\text{eff}} = 2d\epsilon P \,\text{sech}a - (\Lambda + 2d\epsilon)P + \frac{P^2}{2^{d+1}} \frac{\cosh^d(2a)\sinh^d(a)}{\cosh^{3d}(a)}, \tag{3.9}$$

where the power $P = \sum_n u_n^2$ can be evaluated as

$$P = A^2 \coth^d(a). \tag{3.10}$$

From Eq. (3.9) and the extremization conditions of this effective Lagrangian:

$$\frac{\partial \mathcal{L}_{\text{eff}}}{\partial P} = \frac{\partial \mathcal{L}_{\text{eff}}}{\partial a} = 0, \tag{3.11}$$

one can obtain the $P = P(\Lambda)$ (in any dimension, and for different values of ϵ).

One can compare the results of Eq. (3.11) with direct numerical computations identifying the ground state solutions of the DNLS equation (again, in any dimension). As relevant examples, we present in Fig. 3.1 the cases of $d = 2$ that we focus on in this chapter, but also for comparison those of $d = 1, 3$. The power of the solutions is given as a function of Λ (for $\epsilon = 1$) in Fig. 3.1. One of the key observations of the figure is the difference in the stationary state properties between the case of $d = 1$ (so-called subcritical case) and the cases of $d = 2$ (critical) and $d = 3$ (supercritical). In fact, as was originally demonstrated in the work of [11], through scaling arguments, and was later proved more rigorously in [12] (see also the recent discussion of [13]), for dimensions larger than the critical dimension (which is given by $d\sigma = 2$ for nonlinearities $|u|^{2\sigma}u$), there is a *power threshold* for the excitation of localized solitary waves. That is, contrary to what is the case for one dimension such excitations where there is such a solution *for any value of the power*, for higher dimensional problems, such a solution exists *only* for powers $P \geq P_{cr}$, where P_{cr} denotes the relevant threshold.

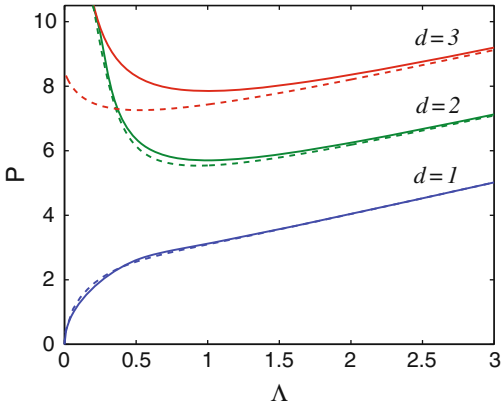

Fig. 3.1 The plot shows the one-, two-, and three-dimensional results for the power P of the stationary solutions for different Λ in Eq. (3.6). The *solid lines* denote the full numerical results, while the *dashed* ones the results of the variational approximation described in the text

Another important comment to make here concerns the accuracy of the variational approximation in characterizing the stationary solutions. We can see that in the one- and two-dimensional settings, the VA is fairly accurate in capturing the trends of the full numerical solution, however, in the three-dimensional context it clearly misses in its quantitative description (although it does share some qualitative trends with the actual solution). As an example, we note that in that case, the minimum power occurs for $\Lambda \approx 1$ in the numerical results, while it happens for $\Lambda \approx 0.5234$ in the variational approximation.

The existence of the power thresholds discussed above also bears important information for the stability of the localized solutions of the discrete model. In particular, as discussed in the previous chapter and as stems from the original work of [6–8] and later from the work of [9, 10], the change of monotonicity of the $P = P(\Lambda)$ curve has an important consequence in the stability of the structure, in particular, the single-humped solution is stable when $dP/d\Lambda > 0$, while it is unstable due to a real eigenvalue pair when $dP/d\Lambda < 0$. Hence, as the continuum limit is approached through decreasing Λ (or equivalently through increasing ϵ), the originally stable discrete single-humped soliton has to become unstable, and this happens precisely at the point where $dP/d\Lambda = 0$. This instability was observed in [14] and the relevant criterion was originally proposed in the work of Vakhitov and Kolokolov and therefore is often referred to as the VK criterion [12].

In Fig. 3.2, we show two examples of the relevant solution, as obtained numerically, one deeply in the discrete regime for $\Lambda = 1.5$ (linearly stable) and one very close to the continuum regime for $\Lambda = 0.05$ (linearly unstable, since $\Lambda < \epsilon = 1$). The figure also shows the corresponding spectral planes (λ_r, λ_i) of the relevant linearization eigenvalues $\lambda = \lambda_r + i\lambda_i$, verifying the stability of the former and instability of the latter (due to a real eigenvalue pair). Note how the latter solution appears to approach its radially symmetric continuum limit (the Townes soliton of [2]). It should also be pointed out in that regard that as $\Lambda \to 0$ (see also the relevant trend in Fig. 3.1), the squared l^2 norm of the solution can be seen to approach $P \approx 11.7$ which is the well-known critical mass of the Townes solution [13].

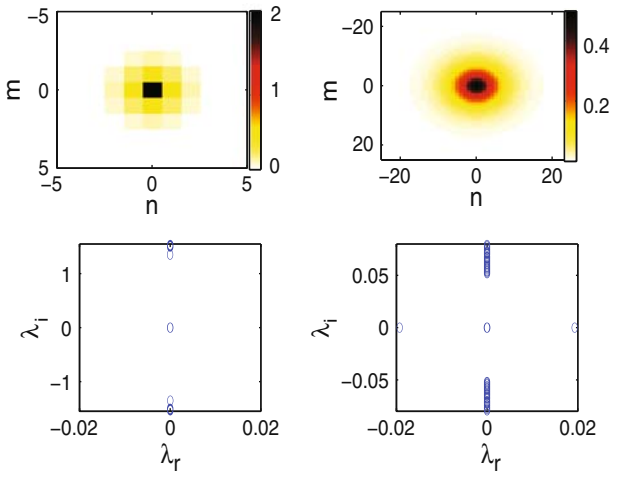

Fig. 3.2 The *top left panel* shows a contour plot of the fundamental solution of the two-dimensional DNLS for $\Lambda = 1.5$, while the *top right* shows the same solution for $\Lambda = 0.05$ (when it approaches its continuum profile). The former solution is stable as is shown in the *bottom left panel* illustrating the spectral plane (λ_r, λ_i) of its linearization eigenvalues $\lambda = \lambda_r + i\lambda_i$, while the latter solution is unstable (having $\Lambda < 1$), as is shown in the *bottom right panel*

In closing, it would be interesting to highlight one important open problem arising in the computations of this fundamental solution for $d = 2$ and 3. In particular, our numerical results indicate that for such solutions, the instability due to the sign change of $dP/d\Lambda$ occurs *precisely* at $\Lambda = 1$ (or, when ϵ is present in the equation, when $\Lambda = \epsilon$). Hence, a relevant mathematical question arises as to whether indeed for dimensions $d \geq 2$, one can more precisely quantify the location of the instability and whether in particular it indeed occurs for $\Lambda = \epsilon$ more generally or not. This is a conjecture that it would be worthwhile to settle.

One direction toward proving this conjecture is to try to derive properties based on Eq. (3.6), connecting the power of the solution P, the frequency Λ, and the coupling strength ϵ. Such a property can be obtained, e.g., by multiplying (3.6) by u_n and summing over n, resulting in the identity

$$(2d\epsilon + \Lambda)P = 2\epsilon L + N, \tag{3.12}$$

where $L = \sum_n \sum_j u_{n+e_j} u_n$ and $N = \sum_n u_n^4$. Similarly, multiplying Eq. (3.6) by $\partial u_n/\partial\Lambda$ and summing over n, along with using Eq. (3.12), one can also derive the identity

$$P = \frac{1}{2}\frac{dN}{d\Lambda}. \tag{3.13}$$

Unfortunately, in addition to Eqs. (3.12) and (3.13), one needs one more equation to eliminate both N and L and derive the dependence of P on ϵ and Λ that would permit an explicit calculation of the relevant critical point $dP/d\Lambda = 0$.

3.3 Multipulses and Discrete Vortices

We now try to address the existence of more complex multisite structures, starting from the AC limit of $\epsilon = 0$ in Eq. (3.6). Note that similarly to our one-dimensional exposition of the previous chapter, for notational simplicity, we set $\Lambda = 1$ in what follows. Our discussion will closely follow [14].

3.3.1 Formulation of the Bifurcation Problem Near $\epsilon = 0$

The relevant stationary equation of interest then reads

$$\left(1 - |v_{n,m}|^2\right)\phi_{n,m} = \epsilon\left(v_{n+1,m} + v_{n-1,m} + v_{n,m+1} + v_{n,m-1}\right). \tag{3.14}$$

In the $\epsilon = 0$, similarly to the one-dimensional case, the solutions of this equation can be fully characterized

$$v_{n,m}^{(0)} = \begin{cases} e^{i\theta_{n,m}}, & (n,m) \in S, \\ 0, & (n,m) \in \mathbb{Z}^2 \backslash S, \end{cases} \tag{3.15}$$

where S is a finite set of nodes on the lattice and $\theta_{n,m}$ are parameters for these *excited sites*. Since θ_0 is arbitrary, we can set $\theta_{n_0,m_0} = 0$ for a particular node $(n_0, m_0) \in S$. Using this convention, we can define two special types of localized modes, called discrete solitons and vortices.

The localized solution of the difference equations (3.14) with $\epsilon > 0$ is called a *discrete soliton* when it has all real-valued amplitudes $v_{n,m}$, $\forall (n,m) \in S$ and at the limit (3.15), $\theta_{n,m} = \{0, \pi\}$ for $(n,m) \in S$. On the other hand, if S is a simple closed discrete contour on the plane and the localized solution has complex valued $v_{n,m}$ that satisfies the limit (3.15) with $\theta_{n,m} \in [0, 2\pi]$, $(n,m) \in S$, then we call such a solution a *discrete vortex*.

Discrete vortices can be partitioned into symmetric and asymmetric ones as follows. If S is a simple closed discrete contour on the plane, such that each node $(n,m) \in S$ has exactly two adjacent nodes in vertical or horizontal directions along S. Let $\Delta\theta_j$ be the phase difference between two successive nodes in the contour S, defined according to the enumeration $j = 1, 2, \ldots, \dim(S)$, such that $|\Delta\theta_j| \leq \pi$. If the phase differences $\Delta\theta_j$ are constant along S, the discrete vortex is called symmetric. Otherwise, it is called asymmetric. The total number of 2π phase shifts across the closed contour S is called the vortex charge. More specifically, we consider discrete contours

$$S_M = \{(1,1),(2,1),\ldots,(M+1,1),(M+1,2),\ldots,(M+1,M+1),$$
$$(M,M+1),\ldots,(1,M+1),(1,M),\ldots,(1,2)\}, \tag{3.16}$$

containing $4M$ sites. Given the above definition, the contour S_M for a fixed M could support symmetric and asymmetric vortices with some charge L. Arguably, the simplest vortex is the symmetric charge-one vortex cell ($M = L = 1$: $\theta_{1,1} = 0$, $\theta_{2,1} = \pi/2$, $\theta_{2,2} = \pi$, $\theta_{1,2} = 3\pi/2$) [16, 29]. Although the main formalism below is developed for any $M \geq 1$, we obtain a complete set of results on persistence and stability of discrete vortices only in the cases $M = 1, 2, 3$, which are of most physical interest.

It then follows directly from the general method [17] that the discrete solitons of the two-dimensional NLS lattice (3.14) can be continued for $0 < \epsilon < \epsilon_0$ for some $\epsilon_0 > 0$. It is more complicated to find a configuration of $\theta_{n,m}$ for $(n,m) \in S$ that allows us to continue the discrete vortices for $\epsilon > 0$. The continuation of the discrete solitons and vortices is based on the Implicit Function Theorem and the Lyapunov–Schmidt Reduction Theorem [18, 19].

We denote by $\mathcal{O}(0)$ a small neighborhood of $\epsilon = 0$, such that $\mathcal{O}(0) = (-\epsilon_0, \epsilon_0)$ for some $\epsilon_0 > 0$. Let $N = \dim(S)$ and $\mathcal{T}$ be the torus on $[0, 2\pi]^N$, such that $\theta_{n,m}$ for $(n,m) \in S$ form a vector $\boldsymbol{\theta} \in \mathcal{T}$. Let $\Omega = L^2(\mathbb{Z}^2, \mathbb{C})$ be the Hilbert space of square-summable complex-valued sequences $\{\phi_{n,m}\}_{(n,m)\in\mathbb{Z}^2}$, equipped with the standard inner product and l^2 norm.

It can then be proved that there exists a unique (discrete soliton) solution of the difference equations (3.14) in the domain $\epsilon \in \mathcal{O}(0)$ with a real profile satisfying $\lim_{\epsilon\to 0} v_{n,m} = v^{(0)}_{n,m}$, and $v^{(0)}_{n,m}$ is given by (3.15) with $\theta_{n,m} = \{0, \pi\}$, $(n,m) \in S$. The solution is analytic in ϵ in this neighborhood. This can be proved by considering the equations for the stationary solution of Eq. (3.14) as the zeros of a vector valued function $f_{n,m}$. Then this mapping has a bounded and continuous Fréchet derivative

$$\mathcal{L}_{n,m} = \left(1 - 3v^2_{n,m}\right) - \epsilon\left(s_{+1,0} + s_{-1,0} + s_{0,+1} + s_{0,-1}\right), \tag{3.17}$$

where $s_{n',m'}$ is the shift operator, such that $s_{n',m'}u_{n,m} = u_{n+n',m+m'}$. The kernel of $\mathcal{L}_{n,m}$ is empty for $\epsilon = 0$. Therefore, for $\epsilon = 0$, $\mathcal{L}^{(0)}_{n,m}$ has a bounded inverse, which implies by the implicit function theorem (see Appendix 1 in [19] and Chap. 2.2 in [18]) that there is a continuous (in fact, analytic) in ϵ solution $v_{n,m}(\epsilon)$ in our case.

Now for a general profile $v^{(0)}_{n,m}$ at the AC limit, the continuation of such a solution for $\epsilon \in \mathcal{O}(0)$ requires that some conditions, constituting a vector valued function which we will denote by $\mathbf{g}(\boldsymbol{\theta}, \epsilon)$, be satisfied. Moreover, the function $\mathbf{g}(\boldsymbol{\theta}, \epsilon)$ is analytic in $\epsilon \in \mathcal{O}(0)$ and $\mathbf{g}(\boldsymbol{\theta}, 0) = \mathbf{0}$ for any $\boldsymbol{\theta}$. This can be shown for a general solution $v_{n,m}$, by considering the vector equations (3.14) and their complex conjugate (denote the vector valued function by $\mathbf{f}(\mathbf{v}, \bar{\mathbf{v}}, \epsilon)$). Then, taking the Fréchet derivative of $\mathbf{f}(\boldsymbol{v}, \bar{\boldsymbol{v}}, \epsilon)$ with respect to $\boldsymbol{v}$ and $\bar{\boldsymbol{v}}$, we compute the linearization operator $\mathcal{H}$ for the difference Eq. (3.14):

$$\mathcal{H}_{n,m} = \begin{pmatrix} 1-2|v_{n,m}|^2 & -v_{n,m}^2 \\ -\bar{v}_{n,m}^2 & 1-2|v_{n,m}|^2 \end{pmatrix} - \epsilon \left(s_{+1,0} + s_{-1,0} + s_{0,+1} + s_{0,-1}\right) \begin{pmatrix} 1 & 0 \\ 0 & 1 \end{pmatrix}. \tag{3.18}$$

Let $\mathcal{H}^{(0)} = \mathcal{H}(\boldsymbol{\phi}^{(0)}, 0)$. Note that dim ker$(\mathcal{H}^{(0)}) = N$. Moreover, eigenvectors of ker$(\mathcal{H}^{(0)})$ re-normalize the parameters $\theta_{n,m}$ for $(n,m) \in S$ in the limiting solution (3.15). By the Lyapunov Reduction Theorem [19, Chap. 7.1], there exists a decomposition $\Omega = \text{ker}(\mathcal{H}^{(0)}) \oplus \omega$, such that $\mathbf{g}(\boldsymbol{\theta}, \epsilon)$ is defined in terms of the projections to ker$(\mathcal{H}^{(0)})$. Let $\{\mathbf{e}_{n,m}\}_{(n,m)\in S}$ be a set of N linearly independent eigenvectors in the kernel of $\mathcal{H}^{(0)}$. It follows from the representation,

$$\mathcal{H}_{n,m}^{(0)} = -\begin{pmatrix} 1 & e^{2i\theta_{n,m}} \\ e^{-2i\theta_{n,m}} & 1 \end{pmatrix}, \quad (n,m) \in S \tag{3.19}$$

that each eigenvector $\mathbf{e}_{n,m}$ in the set $\{\mathbf{e}_{n,m}\}_{(n,m)\in S}$ has the only non-zero element $(e^{i\theta_{n,m}}, -e^{-i\theta_{n,m}})^T$ at the (n,m)th position of $(\mathbf{u}, \mathbf{w}) \in \Omega \times \Omega$. By projections of the nonlinear equations to ker$(\mathcal{H}^{(0)})$, we derive an implicit representation for the functions $\mathbf{g}(\boldsymbol{\theta}, \epsilon)$:

$$\begin{aligned}(n,m) \in S: \; 2i g_{n,m}(\boldsymbol{\theta}, \epsilon) = {} & (1-|v_{n,m}|^2)\left(e^{-i\theta_{n,m}} v_{n,m} - e^{i\theta_{n,m}} \bar{v}_{n,m}\right) \\ & - \epsilon e^{-i\theta_{n,m}} \left(v_{n+1,m} + v_{n-1,m} + v_{n,m+1} + v_{n,m-1}\right) \\ & + \epsilon e^{i\theta_{n,m}} \left(\bar{v}_{n+1,m} + \bar{v}_{n-1,m} + \bar{v}_{n,m+1} + \bar{v}_{n,m-1}\right), \end{aligned} \tag{3.20}$$

where the factor $(2i)$ is introduced for convenience. By setting $v_{n,m} = e^{i\theta_{n,m}} \phi_{n,m}$ for $(n,m) \in S$ and renaming $\phi_{n,m} \to v_{n,m}$ we end up obtaining the solvability conditions

$$\begin{aligned}(n,m) \in S: \; -2i g_{n,m}(\boldsymbol{\theta}, \epsilon) = {} & \epsilon e^{-i\theta_{n,m}} \left(v_{n+1,m} + v_{n-1,m} + v_{n,m+1} + v_{n,m-1}\right) \\ & - \epsilon e^{i\theta_{n,m}} \left(\bar{v}_{n+1,m} + \bar{v}_{n-1,m} + \bar{v}_{n,m+1} + \bar{v}_{n,m-1}\right). \end{aligned} \tag{3.21}$$

Note that these are the same conditions to leading order to the solvability conditions directly inferred by Eq. (3.14), by multiplying the equation by $\bar{v}_{n,m}$ and subtracting the complex conjugate, namely

$$\begin{aligned}(n,m) \in S: \; -2i g_{n,m}(\boldsymbol{\theta}, \epsilon) = {} & \epsilon \bar{v}_{n,m} \left(v_{n+1,m} + v_{n-1,m} + v_{n,m+1} + v_{n,m-1}\right) \\ & - \epsilon v_{n,m} \left(\bar{v}_{n+1,m} + \bar{v}_{n-1,m} + \bar{v}_{n,m+1} + \bar{v}_{n,m-1}\right). \end{aligned} \tag{3.22}$$

Note, also, that given the analyticity of these solvability conditions, they can be Taylor expanded in ϵ, and so can the solution $v_{n,m}$. Furthermore, in this reformulation

of the problem for the angles $\theta_{m,n}$ (as a function of ϵ), the gauge or U(1) invariance of the original problem can be translated into a shift of the angle $\theta_{n,m} \to \theta_{n,m} + \theta_0$, which yields a one parameter family of roots of $\mathbf{g}(\boldsymbol{\theta}, \epsilon)$. This implies that the Jacobian matrix $(\mathcal{M}_1)_{jk} = \partial g_j^{(1)}/\partial\theta_k$ of the first-order expansion $g^{(1)}$ will have a non-empty kernel with an eigenvector $\mathbf{p}_0 = (1, 1, \ldots, 1)$ due to the gauge transformation. However, if we let X_0 be the constrained subspace of $\mathbb{C}^N$:

$$X_0 = \{\mathbf{u} \in \mathbb{C}^N : \ (\mathbf{p}_0, \mathbf{u}) = 0\}. \tag{3.23}$$

and the matrix $\mathcal{M}_1$ is non-singular in the subspace X_0, then there exists a unique (modulo the shift) analytic continuation of the root of the bifurcation equations for $\epsilon \in \mathcal{O}(0)$ by the Implicit Function Theorem, applied to the nonlinear equation $\mathbf{g}(\boldsymbol{\theta}, \epsilon) = \mathbf{0}$ [19, Appendix 1].

An important generalization of the above continuation is the following (regarding conditions under which a solution family cannot be continued for $\epsilon \in \mathcal{O}(0)$: let $\boldsymbol{\theta}_*$ be a $(1 + d)$-parameter solution of $\mathbf{g}^{(1)}(\boldsymbol{\theta}) = \mathbf{0}$ and $\mathcal{M}_1$ have a zero eigenvalue of multiplicity $(1 + d)$, where $1 \leq d \leq N - 1$. Let $\mathbf{g}^{(2)}(\boldsymbol{\theta}_*) = \cdots = \mathbf{g}^{(K-1)}(\boldsymbol{\theta}_*) = \mathbf{0}$ but $\mathbf{g}^{(K)}(\boldsymbol{\theta}_*) \neq \mathbf{0}$. The limiting solution (3.15) can be continued in the domain $\epsilon \in \mathcal{O}(0)$ only if $\mathbf{g}^{(K)}(\boldsymbol{\theta}_*)$ is orthogonal to $\ker(\mathcal{M}_1)$. If $\mathbf{g}^{(K)}(\boldsymbol{\theta}_*) \notin X_d$, where

$$X_d = \{\mathbf{u} \in X_0 : \ (\mathbf{p}_l, \mathbf{u}) = 0, \ l = 1, \ldots, d\}, \tag{3.24}$$

then the solution can not be continued in $\epsilon \in \mathcal{O}(0)$, according to Chap. 1.3 of [19].

3.3.2 Persistence of Discrete Solutions

We now consider discrete soliton and vortex solutions over the contours S_M and order the angles of which the contour consists as $\theta_1, \theta_2, \ldots, \theta_N$. Given the nature of the considered (closed, square) contours, periodic boundary conditions are applied ($\theta_0 = \theta_N, \theta_1 = \theta_{N+1}$). As per the definition above, a discrete vortex has the charge L if the phase difference $\Delta\theta_j$ between two successive nodes changes by $2\pi L$ along the discrete contour S_M, where $\Delta\theta_j$ is defined within the fundamental branch $|\Delta\theta_j| \leq \pi$. By gauge transformation, we can always set $\theta_1 = 0$ for convenience. We will also choose $\theta_2 = \theta$ with $0 \leq \theta \leq \pi$ for convenience, which corresponds to discrete vortices with $L \geq 0$ (the existence and stability of their negative charge counterparts is the same).

To identify the leading order persistence conditions, we substitute the limiting AC solution $v_{n,m}^{(0)}$ solution in the bifurcation equations to obtain $g^{(1)}$ in the form

$$\mathbf{g}_j^{(1)}(\boldsymbol{\theta}) = \sin\left(\theta_j - \theta_{j+1}\right) + \sin\left(\theta_j - \theta_{j-1}\right), \qquad 1 \leq j \leq N. \tag{3.25}$$

The bifurcation equations $\mathbf{g}^{(1)}(\boldsymbol{\theta}) = \mathbf{0}$ are rewritten as a system of N nonlinear equations for N parameters θ_1,θ_2,...,θ_N as follows:

$$\sin(\theta_2 - \theta_1) = \sin(\theta_3 - \theta_2) = \cdots = \sin(\theta_N - \theta_{N-1}) = \sin(\theta_1 - \theta_N). \qquad (3.26)$$

These types of conditions also arose in the work of [20, 21]. We now attempt to classify all solutions of the bifurcation equations.

If we let $a_j = \cos(\theta_{j+1} - \theta_j)$ for $1 \le j \le N$, such that $\theta_1 = 0$, $\theta_2 = \theta$, and $\theta_{N+1} = 2\pi L$, where $N = 4M$, $0 \le \theta \le \pi$ and L is the vortex charge. All solutions of the bifurcation equations (3.26) reduce to the following four families:

(i) discrete solitons with $\theta = \{0, \pi\}$ and

$$\theta_j = \{0, \pi\}, \qquad 3 \le j \le N, \qquad (3.27)$$

such that the set $\{a_j\}_{j=1}^N$ includes l coefficients $a_j = 1$ and $N - l$ coefficients $a_j = -1$, where $0 \le l \le N$.

(ii) symmetric vortices of charge L with $\theta = \pi L/2M$, where $1 \le L \le 2M - 1$, and

$$\theta_j = \frac{\pi L(j-1)}{2M}, \qquad 3 \le j \le N, \qquad (3.28)$$

such that all N coefficients are the same: $a_j = a = \cos(\pi L/2M)$.

(iii) one-parameter families of asymmetric vortices of charge $L = M$ with $0 < \theta < \pi$ and

$$\theta_{j+1} - \theta_j = \left\{ \begin{array}{c} \theta \\ \pi - \theta \end{array} \right\} \ \mathrm{mod}(2\pi), \qquad 2 \le j \le N, \qquad (3.29)$$

such that the set $\{a_j\}_{j=1}^N$ includes $2M$ coefficients $a_j = \cos\theta$ and $2M$ coefficients $a_j = -\cos\theta$.

(iv) zero-parameter asymmetric vortices of charge $L \neq M$ and

$$\theta = \theta_* = \frac{\pi}{2}\left(\frac{n + 2L - 4M}{n - 2M}\right), \qquad 1 \le n \le N - 1, \quad n \neq 2M, \qquad (3.30)$$

such that the set $\{a_j\}_{j=1}^N$ includes n coefficients $a_j = \cos\theta_*$ and $N - n$ coefficients $a_j = -\cos\theta_*$ and the family (iv) does not reduce to any of the families (i)–(iii).

This can be seen because essentially there are only two roots of the sine function that permit simultaneously satisfying the bifurcation equations. These are the choices of Eq. (3.29), leading, respectively, to either $a_j = \cos(\theta)$ or to $a_j = -\cos(\theta)$. If we generically assume that there are totally n choices of the former type and $N - n$ ones of the latter type within the contour, then

$$\theta_{N+1} = n\theta + (N - n)(\pi - \theta) = (2n - N)\theta + (N - n)\pi = 2\pi L,$$

where L is the integer charge of the discrete vortex. There are only two solutions of the above equation. When θ is arbitrary parameter, we have $n = N/2 = 2M$ and $L = M$, which gives the one-parameter family (iii). When $\theta = \theta_*$ is fixed, we have

$$\theta_* = \frac{\pi}{2}\left(\frac{n + 2L - 4M}{n - 2M}\right).$$

When $n = N - 2L$, we have the family (i) with $N - 2L$ phases $\theta_j = 0$ and $2L$ phases $\theta_j = \pi$. Since the charge is not assigned to discrete solitons, the parameter L could be half-integer: $L = (N - l)/2$, where $0 \le l \le N$. When $n = 4M$, we have the family (ii) for any $1 \le L \le 2M - 1$. Other choices of n, which are irreducible to the families (i)–(iii), produce the family (iv). Furthermore, it is worthwhile to note that there are special cases where family (iii) reduces to families (ii) and (i); these will be dubbed supersymmetric cases. In particular, when $\theta = 0$ and π, the family (iii) reduces to the family (i) with $l = 2M$. When $\theta = \pi/2$, the family (iii) reduces to the family (ii) with $L = M$. We shall call the corresponding solutions of family (i) the supersymmetric soliton and of family (ii) the supersymmetric vortex.

One can make a simple combinatorial enumeration of the solutions of families (i)–(iii). In the case of (i), there are $N_1 = 2^{N-1}$, since aside from the first site, all others can be either 0 or π. There are also $N_2 = 2M - 1$ solutions of family (ii), and N_3 solutions of family (iii), where

$$N_3 = 2^{N-1} - \sum_{k=0}^{2M-1} \frac{N!}{k!(N-k)!}. \tag{3.31}$$

As special case examples that will be of relevance to our discussion below, we mention the contours with $M = 1$ (four sites) and $M = 2$ (eight sites). In the first case, there are eight solutions of type (i), one of type (ii), three solutions of type (iii), and no solutions of the family (iv). The three one-parameter asymmetric solutions are

$$\text{(a)}\ \ \theta_1 = 0,\ \theta_2 = \theta,\ \theta_3 = \pi,\ \theta_4 = \pi + \theta, \tag{3.32}$$

$$\text{(b)}\ \ \theta_1 = 0,\ \theta_2 = \theta,\ \theta_3 = 2\theta,\ \theta_4 = \pi + \theta, \tag{3.33}$$

$$\text{(c)}\ \ \theta_1 = 0,\ \theta_2 = \theta,\ \theta_3 = \pi,\ \theta_4 = 2\pi - \theta. \tag{3.34}$$

Similarly in the case with $M = 2$, there are 128 solutions of family (i), 3 solutions of family (ii), 35 solutions of family (iii), and 14 of family (iv). The three symmetric vortices have charge $L = 1$ ($\theta = \pi/4$), $L = 2$ ($\theta = \pi/2$), and $L = 3$ ($\theta = 3\pi/4$). The one-parameter asymmetric vortices include 35 combinations of 4 upper choices and 4 lower choices in (3.29). Finally, the zero parameter asymmetric vortices include seven combinations of vortices with $L = 1$ for seven phase differences $\pi/6$

and one phase difference $5\pi/6$ and seven combinations of vortices with $L = 3$ for one phase difference $\pi/6$ and seven phase differences $5\pi/6$.

3.3.2.1 First-Order Reductions

The Jacobian $\mathcal{M}_1$ of the first-order bifurcation equations $\mathbf{g}^{(1)}(\boldsymbol{\theta})$ can be obtained from Eq. (3.25) as

$$(\mathcal{M}_1)_{i,j} = \begin{cases} \cos(\theta_{j+1} - \theta_j) + \cos(\theta_{j-1} - \theta_j), & i = j, \\ -\cos(\theta_j - \theta_i), & i = j \pm 1, \\ 0, & |i - j| \geq 2, \end{cases} \tag{3.35}$$

subject to the periodic boundary conditions. It is interesting that this is the same type of structure as we encountered in the one-dimensional configurations of the previous chapter, and it is the one also encountered in the perturbation theory of continuous multipulse solitons in coupled NLS equations [20].

If we let n_0, z_0, and p_0 be the numbers of negative, zero, and positive terms of $a_j = \cos(\theta_{j+1} - \theta_j)$, $1 \leq j \leq N$ (therefore $n_0 + z_0 + p_0 = N$), it is important based on this information to infer how many eigenvalues of $\mathcal{M}_1$ are negative, zero, or positive. Assuming $z_0 = 0$ (note that this is not true in supersymmetric cases), it turns out (see the appendix of [20] for a relevant proof by induction arguments) that the eigenvalues are intimately connected with the quantity

$$A_1 = \sum_{i=1}^{N} \prod_{j \neq i} a_j = \left(\prod_{i=1}^{N} a_i \right) \left(\sum_{i=1}^{N} \frac{1}{a_i} \right). \tag{3.36}$$

In particular, as expected there exists a zero eigenvalue in $\mathcal{M}_1$ due to the gauge invariance. Therefore, denoting the characteristic polynomial of $\mathcal{M}_1$ as $D(\lambda)$, it is clear that $D(0) = 0$. It is then important to evaluate $D'(0) = -\lambda_1 \lambda_2 \ldots \lambda_{N-1}$. A key result in that regard is that for this matrix $D'(0) = -NA_1$; therefore, an immediate consequence is that if $A_1 \neq 0$, then the multiplicity of the zero eigenvalue is $z(\mathcal{M}_1) = 1$. If $A_1 = 0$, then $z(\mathcal{M}_1) \geq 2$. Note also that from the above results (comparing $D'(0)$) $(-1)^{n(\mathcal{M}_1)} = \text{sign}(A_1)$, where $n(\mathcal{M}_1)$ denotes the number of negative eigenvalues of the matrix; this implies that $n(\mathcal{M}_1)$ is even if $A_1 > 0$ and is odd if $A_1 < 0$. Finally, if $p(\mathcal{M}_1)$ will be used to denote the number of positive eigenvalues, then as indicated in [20], there are two possible scenario (if $A_1 \neq 0$) for the related eigenvalues: either $n(\mathcal{M}_1) = n_0 - 1$, $p(\mathcal{M}_1) = p_0$ or $n(\mathcal{M}_1) = n_0$, $p(\mathcal{M}_1) = p_0 - 1$.

In some important special cases (for what follows), the eigenvalues of the matrix can be computed analytically. More specifically,if all coefficients $a_j =$

$\cos(\theta_{j+1} - \theta_j)$, $1 \le j \le N$ are equal $a_j = a$, then, the eigenvalues of the matrix can be computed as

$$\lambda_n = 4a \sin^2 \frac{\pi n}{N}, \qquad 1 \le n \le N. \tag{3.37}$$

This is straightforward to see since the eigenfunction equation becomes

$$a\left(2x_j - x_{j+1} - x_{j-1}\right) = \lambda x_j, \qquad x_0 = x_N,\ x_1 = x_{N+1}, \tag{3.38}$$

which is solvable by the using the discrete Fourier modes $x_j = \exp(i(2\pi jn/N))$ for $1 \le j, n \le N$, yielding the above eigenvalue expression.

On the other hand, if the elements of the matrix alternate in sign $a_j = (-1)^j a$, $1 \le j \le 4M$, then the eigenvalue problem can be written as a system of two coupled linear difference equations of the form

$$a\left(y_j - y_{j-1}\right) = \lambda x_j, \qquad a\left(x_j - x_{j+1}\right) = \lambda y_j, \qquad 1 \le j \le 2M, \tag{3.39}$$

subject to the periodic boundary conditions: $x_1 = x_{2M+1}$ and $y_0 = y_{2M}$. Once again, the discrete Fourier transform can be used according to $x_j = x_0 \exp(i(2\pi jn/2M))$ and $y_j = y_0 \exp(i(2\pi jn/2M))$ for $1 \le j, n \le 2M$ and this yields the eigenvalues

$$\lambda_n = -\lambda_{n+2M} = 2a \sin \frac{\pi n}{2M}, \qquad 1 \le n \le 2M, \tag{3.40}$$

such that $n(\mathcal{M}_1) = 2M - 1$, $z(\mathcal{M}_1) = 2$, and $p(\mathcal{M}_1) = 2M - 1$. These numbers do not change if the set $\{a_j\}_{j=1}^N$ is obtained from the sign-alternating set $\{(-1)^j a\}_{j=1}^N$ by permutations (see [14] for a proof of the last statement).

The above results indicate that discrete solitons can be typically continued uniquely for finite ϵ, since $z(\mathcal{M}_1) = 1$. This is with the notable exception of supersymmetric solitons where the number of positive and negative a_j's is equal. On the other hand, for family (ii), all coefficients a_j are the same: $a_j = a = \cos(\pi L/2M)$, $1 \le j \le N$. The above calculation for equal a_j's yields the presence of a zero eigenvalue λ_N; the remaining $(N-1)$ eigenvalues are all positive for $a > 0$ (when $1 \le L \le M - 1$), negative for $a < 0$ (when $M + 1 \le L \le 2M - 1$), and zero for $a = 0$ (in the supersymmetric case of $L = M$). Therefore, states other than the supersymmetric ones are also guaranteed to have a unique continuation also in the case of discrete *symmetric* vortices. The first-order reductions are less informative in the case of asymmetric discrete vortices of family (iii), whereby there are $2M$ coefficients $a_j = \cos\theta$ and $2M$ coefficients $a_j = -\cos\theta$, which are non-zero for $\theta \neq \pi/2$. The count of eigenvalues of the matrix $\mathcal{M}_1$ yields $n(\mathcal{M}_1) = 2M - 1$, $z(\mathcal{M}_1) = 2$, and $p(\mathcal{M}_1) = 2M - 1$. Therefore in this case, the higher multiplicity of the zero eigenvalue (related, at heart, with the additional freedom in the selection of the angular parameter θ) leads to an inconclusive result for such solutions. Lastly, for family (iv), the fact that $A_1 \neq 0$, again preserves the zero eigenvalue multiplicity

as $z(\mathcal{M}_1) = 1$, permitting a unique continuation of such zero parameter asymmetric vortices.

3.3.2.2 Second-Order Reductions

To determine the fate of supersymmetric solitons and vortices, as well as that of mono-parametric, asymmetric vortices, we now expand the bifurcation function $\mathbf{g}(\boldsymbol{\theta}, \epsilon)$ to second order. Starting with the first-order correction in the solution, we have

$$\left(1 - 2|v_{n,m}^{(0)}|^2\right) v_{n,m}^{(1)} - v_{n,m}^{(0)2} \bar{v}_{n,m}^{(1)} = v_{n+1,m}^{(0)} + v_{n-1,m}^{(0)} + v_{n,m+1}^{(0)} + v_{n,m-1}^{(0)}. \tag{3.41}$$

To solve this more complicated equation, we will distinguish the cases of the different contours; we will consider, in particular, the contours with $M = 1$, $M = 2$, and $M \geq 3$.

In the case of $M = 1$, the inhomogeneous equation (3.41) has a solution of the form

$$v_{n,m}^{(1)} = -\frac{1}{2}\left[\cos\left(\theta_{j-1} - \theta_j\right) + \cos\left(\theta_{j+1} - \theta_j\right)\right] e^{i\theta_j}, \tag{3.42}$$

for sites in the contour S_M, while for their non-contour neighbors,

$$v_{n,m}^{(1)} = e^{i\theta_j} \tag{3.43}$$

and every other site vanishes at this order. Substituting this first order correction within the bifurcation equations to deduce $\mathbf{g}^{(2)}(\boldsymbol{\theta})$, we find the form

$$\begin{aligned} \mathbf{g}_j^{(2)}(\boldsymbol{\theta}) = &\frac{1}{2}\sin\left(\theta_{j+1} - \theta_j\right)\left[\cos(\theta_j - \theta_{j+1}) + \cos\left(\theta_{j+2} - \theta_{j+1}\right)\right] \\ &+ \frac{1}{2}\sin\left(\theta_{j-1} - \theta_j\right)\left[\cos\left(\theta_j - \theta_{j-1}\right) + \cos(\theta_{j-2} - \theta_{j-1})\right], \qquad 1 \leq j \leq N. \end{aligned} \tag{3.44}$$

One can then straightforwardly compute the vector $\mathbf{g}^{(2)}(\boldsymbol{\theta})$ for the asymmetric solutions (3.32), (3.33), and (3.34):

$$\text{(a)}\ \ \mathbf{g}_2 = \begin{pmatrix} 0 \\ 0 \\ 0 \\ 0 \end{pmatrix}, \quad \text{(b)}\ \ \mathbf{g}_2 = \begin{pmatrix} 2 \\ 0 \\ -2 \\ 0 \end{pmatrix} \sin\theta\cos\theta, \quad \text{(c)}\ \ \mathbf{g}_2 = \begin{pmatrix} 0 \\ -2 \\ 0 \\ 2 \end{pmatrix} \sin\theta\cos\theta.$$

The key observation, however, concerns the kernel of $\mathcal{M}_1$, which as illustrated above has a second element (in addition to the gauge invariance eigenvector $(1, 1, 1, 1)^T$). This element is evaluated as

$$\text{(a) } \mathbf{p}_1 = \begin{pmatrix} 0 \\ 1 \\ 0 \\ 1 \end{pmatrix}, \quad \text{(b) } \mathbf{p}_1 = \begin{pmatrix} 0 \\ 1 \\ 2 \\ 1 \end{pmatrix}, \quad \text{(c) } \mathbf{p}_1 = \begin{pmatrix} 0 \\ 1 \\ 0 \\ -1 \end{pmatrix}.$$

The Fredholm alternative $(\mathbf{p}_1, \mathbf{g}_2) = 0$ is satisfied for the solution (a) but fails for the solutions (b) and (c), unless $\theta = \{0, \pi/2, \pi\}$. Therefore, the important conclusion from this exercise is that solutions (b) and (c) *cannot* be continued for $\epsilon \neq 0$.

In the case of $M = 2$, the correction is the same as in the previous case, as given by Eqs. (3.42) and (3.43), except for the central node (2, 2), where contributions from its four neighboring sites yield

$$v^{(1)}_{2,2} = e^{i\theta_2} + e^{i\theta_4} + e^{i\theta_6} + e^{i\theta_8}. \tag{3.45}$$

This, in turn, modifies the entries of the bifurcation function according to

$$\mathbf{g}^{(2)}_j(\boldsymbol{\theta}) \to \mathbf{g}^{(2)}_j(\boldsymbol{\theta}) + \sin(\theta_j - \theta_{j-2}) + \sin(\theta_j - \theta_{j+2}) + \sin(\theta_j - \theta_{j+4}), \quad j = 2, 4, 6, 8. \tag{3.46}$$

In that case, there are 35 one-parameter asymmetric vortex solitons, each of which has a corresponding second eigenvector $\mathbf{p}_1$ in the kernel of $\mathcal{M}_1$. For all but one of these solutions (assuming that $\theta \neq \{0, \pi/2, \pi\}$), the condition for continuation of the solution, namely $(\mathbf{p}_1, \mathbf{g}_2) = 0$ fails, hence the solutions cannot exist. The only solution that can be continued in this case is the one with alternating signs of $a_j = \cos(\theta_{j+1} - \theta_j)$.

Finally, in the case of $M \geq 3$, the first-order corrections to the solution still obey (3.42) and (3.43), except for the four corner nodes (2, 2),$(M, 2)$,(M, M), and $(2, M)$ each of which have two neighbors which lead to

$$v^{(1)}_{n,m} = e^{i\theta_{j-1}} + e^{i\theta_{j+1}}, \qquad j = 1, M+1, 2M+1, 3M+1. \tag{3.47}$$

The correction term $\mathbf{g}^{(2)}(\boldsymbol{\theta})$ is given by (3.45), except for the adjacent entries to the four corner nodes on the contour S_M: (1, 1), (1, $M + 1$), $(M + 1, M + 1)$, and $(M + 1, 1)$, which are modified by

$$\begin{aligned} &\mathbf{g}^{(2)}_j(\boldsymbol{\theta}) \to \mathbf{g}^{(2)}_j(\boldsymbol{\theta}) + \sin(\theta_j - \theta_{j-2}), \qquad j = 2, M+2, 2M+2, 3M+2, \\ &\mathbf{g}^{(2)}_j(\boldsymbol{\theta}) \to \mathbf{g}^{(2)}_j(\boldsymbol{\theta}) + \sin(\theta_j - \theta_{j+2}), \qquad j = M, 2M, 3M, 4M. \end{aligned} \tag{3.48}$$

For any $M \geq 3$, there is a solution of family (iii), where $\mathbf{g}_2 = \mathbf{0}$, which is characterized by the alternating signs of coefficients $a_j = \cos(\theta_{j+1} - \theta_j)$ for $1 \leq j \leq N$. In the case $M = 3$, all other solutions of family (iii) have $(\mathbf{p}_1, \mathbf{g}_2) \neq 0$ and hence terminate at the second-order reductions.

Generalizing the results of this section, we have that all asymmetric vortices of family (iii), except for the sign-alternating set $a_j = \cos(\theta_{j+1} - \theta_j) = (-1)^{j+1}\cos\theta$, $1 \le j \le N$, cannot be continued to $\epsilon \neq 0$ for $M = 1, 2, 3$. The only solution of this type which can be continued has the explicit form

$$\theta_{4j-3} = 2\pi(j-1), \quad \theta_{4j-2} = \theta_{4j-3}+\theta, \quad \theta_{4j-1} = \theta_{4j-3}+\pi, \quad \theta_{4j} = \theta_{4j-3}+\pi+\theta, \tag{3.49}$$

where $1 \le j \le M$ and $0 \le \theta \le \pi$. This solution includes two particular cases of supersymmetric solitons of family (i) for $\theta = 0$ and π and supersymmetric vortices of family (ii) for $\theta = \pi/2$. Continuation of the solution (3.49) must be considered beyond the second-order reductions.

In the case of supersymmetric solitons, and considering the matrix $\mathcal{M}_1 + \epsilon\mathcal{M}_2$, it can be found that the second zero eigenvalue of $\mathcal{M}_1$ bifurcates off zero. As a result, the supersymmetric solutions of family (i) can be uniquely continued to discrete solitons.

On the other hand, we need to consider the Jacobian matrix $\mathcal{M}_2$ and its eigenvalues for discrete supersymmetric vortices of different charges (we consider the cases $M = 1$, $M = 2$, and $M \ge 3$). In the case of $M = 1$, the elements of $\mathcal{M}_2$ are given by

$$(\mathcal{M}_2)_{i,j} = \begin{cases} +1, & i = j, \\ -\dfrac{1}{2}, & i = j \pm 2, \\ 0, & |i - j| \neq 0, 2 \end{cases} \tag{3.50}$$

or explicitly

$$\mathcal{M}_2 = \begin{pmatrix} 1 & 0 & -1 & 0 \\ 0 & 1 & 0 & -1 \\ -1 & 0 & 1 & 0 \\ 0 & -1 & 0 & 1 \end{pmatrix}. \tag{3.51}$$

The matrix $\mathcal{M}_2$ has four eigenvalues: $\lambda_1 = \lambda_2 = 2$ and $\lambda_3 = \lambda_4 = 0$. The two eigenvectors for the zero eigenvalue are $\mathbf{p}_3 = (1, 0, 1, 0)^T$ and $\mathbf{p}_4 = (0, 1, 0, 1)^T$. The eigenvector $\mathbf{p}_4$ corresponds to the derivative of the asymmetric vortex (3.32) with respect to parameter θ, while the eigenvector $\mathbf{p}_0 = \mathbf{p}_3 + \mathbf{p}_4$ corresponds to the shift due to gauge invariance.

In the case of $M = 2$, the second-order Jacobian matrix is given by the form

$$\tilde{\mathcal{M}}_2 = \begin{pmatrix} 1 & 0 & -\frac{1}{2} & 0 & 0 & 0 & -\frac{1}{2} & 0 \\ 0 & 0 & 0 & \frac{1}{2} & 0 & -1 & 0 & \frac{1}{2} \\ -\frac{1}{2} & 0 & 1 & 0 & -\frac{1}{2} & 0 & 0 & 0 \\ 0 & \frac{1}{2} & 0 & 0 & 0 & \frac{1}{2} & 0 & -1 \\ 0 & 0 & -\frac{1}{2} & 0 & 1 & 0 & -\frac{1}{2} & 0 \\ 0 & -1 & 0 & \frac{1}{2} & 0 & 0 & 0 & \frac{1}{2} \\ -\frac{1}{2} & 0 & 0 & 0 & -\frac{1}{2} & 0 & 1 & 0 \\ 0 & \frac{1}{2} & 0 & -1 & 0 & \frac{1}{2} & 0 & 0 \end{pmatrix}. \tag{3.52}$$

The corresponding eigenvalue problem can be decoupled into two linear difference equations with constant coefficients, as follows:

$$\begin{aligned} 2x_j - x_{j+1} - x_{j-1} &= 2\lambda x_j, \qquad j = 1, 2, 3, 4 \\ -2y_{j+2} + y_{j+1} + y_{j-1} &= 2\lambda y_j, \qquad j = 1, 2, 3, 4, \end{aligned}$$

subject to the periodic boundary conditions for x_j and y_j; this can again be solved by discrete Fourier transform, yielding the eigenvalues $\lambda_1 = 1$, $\lambda_2 = 2$, $\lambda_3 = 1$, and $\lambda_4 = 0$; $\lambda_5 = 1$, $\lambda_6 = -2$, $\lambda_7 = 1$, and $\lambda_8 = 0$ (the first four are obtained from the first problem, while the latter four from the second problem). In this case also, there are two eigenvectors with zero eigenvalue, namely $\mathbf{p}_4 = (1, 0, 1, 0, 1, 0, 1, 0)^T$ and $\mathbf{p}_8 = (0, 1, 0, 1, 0, 1, 0, 1)^T$, where the eigenvector $\mathbf{p}_8$ corresponds to the derivative of the asymmetric vortex (3.49) with respect to parameter θ and the eigenvector $\mathbf{p}_0 = \mathbf{p}_4 + \mathbf{p}_8$ corresponds to the shift due to gauge invariance.

Finally, in the case of $M \geq 3$, the Jacobian matrix still resembles that of Eq. (3.50), but now the additional entries stem from the four corner nodes of the contours, namely $(1, 1)$, $(1, M+1)$, $(M+1, M+1)$, and $(M+1, 1)$. The second-order Jacobian in this case reads

$$\tilde{\mathcal{M}}_2 = \mathcal{M}_2 + \Delta\mathcal{M}_2, \tag{3.53}$$

where $\Delta\mathcal{M}_2$ is a rank-four non-positive matrix with the elements

$$(\Delta\mathcal{M}_2)_{i,j} = \begin{cases} -1, & i = j = 2, M, M+2, 2M, 2M+2, 3M, 3M+2, 4M, \\ +1, & i = j-2 = M, 2M, 3M, 4M, \\ +1, & i = j+2 = 2, M+2, 2M+2, 3M+2 \end{cases} \tag{3.54}$$

and all other elements are zeros. The explicit form for the modified matrix $\tilde{\mathcal{M}}_2$ in the case $M = 3$ is

$$\tilde{\mathcal{M}}_2 = \begin{pmatrix}
1 & 0 & -\frac{1}{2} & 0 & 0 & 0 & 0 & 0 & 0 & 0 & -\frac{1}{2} & 0 \\
0 & 0 & 0 & -\frac{1}{2} & 0 & 0 & 0 & 0 & 0 & 0 & 0 & \frac{1}{2} \\
-\frac{1}{2} & 0 & 0 & 0 & \frac{1}{2} & 0 & 0 & 0 & 0 & 0 & 0 & 0 \\
0 & -\frac{1}{2} & 0 & 1 & 0 & -\frac{1}{2} & 0 & 0 & 0 & 0 & 0 & 0 \\
0 & 0 & \frac{1}{2} & 0 & 0 & 0 & -\frac{1}{2} & 0 & 0 & 0 & 0 & 0 \\
0 & 0 & 0 & -\frac{1}{2} & 0 & 0 & 0 & \frac{1}{2} & 0 & 0 & 0 & 0 \\
0 & 0 & 0 & 0 & -\frac{1}{2} & 0 & 1 & 0 & -\frac{1}{2} & 0 & 0 & 0 \\
0 & 0 & 0 & 0 & 0 & \frac{1}{2} & 0 & 0 & 0 & -\frac{1}{2} & 0 & 0 \\
0 & 0 & 0 & 0 & 0 & 0 & -\frac{1}{2} & 0 & 0 & 0 & \frac{1}{2} & 0 \\
0 & 0 & 0 & 0 & 0 & 0 & 0 & -\frac{1}{2} & 0 & 1 & 0 & -\frac{1}{2} \\
-\frac{1}{2} & 0 & 0 & 0 & 0 & 0 & 0 & 0 & \frac{1}{2} & 0 & 0 & 0 \\
0 & \frac{1}{2} & 0 & 0 & 0 & 0 & 0 & 0 & 0 & -\frac{1}{2} & 0 & 0
\end{pmatrix}. \tag{3.55}$$

The computation of the eigenvalues of $\tilde{\mathcal{M}}_2$ again decouples into eigenvalue problems for two 6×6 matrices and the resulting spectra can be computed as

$$\lambda_1 = \lambda_7 = -0.780776, \quad \lambda_2 = \lambda_8 = -0.5, \quad \lambda_3 = \lambda_9 = 0,$$
$$\lambda_4 = \lambda_{10} = 0.5, \quad \lambda_5 = \lambda_{11} = 1.28078, \quad \lambda_6 = \lambda_{12} = 1.5.$$

Just as in the previous two cases, also in this case the matrix has exactly two zero eigenvalues, one of which is related to the derivative of the asymmetric vortex and one of which is related to the shift of the gauge invariance.

3.3.2.3 Higher Order Reductions

Since the family of solutions (3.49) survives up to second-order reductions, one needs to consider higher order reductions in order to examine the potential persistence or non-existence of such solutions. Intuitively speaking, the presence of the arbitrary parameter θ in this family of asymmetric vortices appears not to be supported by the symmetry of the corresponding discrete contour, or that of the original dynamical equation. One therefore has to attempt to algorithmically expand

the considerations of the above subsections to higher orders (as direct calculations become extremely cumbersome), to address the issue. We do so as follows.

Let M be the index of the discrete contour S_M and K be the truncation order of the Lyapunov–Schmidt reduction. We construct a squared domain $(n, m) \in D(M, K)$ which includes $N_0 \times N_0$ lattice nodes, where $N_0 = 2K + M + 1$. Corrections of the power series for a given configuration of $\boldsymbol{\theta}$ in (3.49) solve the set of inhomogeneous equations

$$\mathcal{H}^{(0)} \begin{pmatrix} \boldsymbol{\phi}^{(k)} \\ \bar{\boldsymbol{\phi}}^{(k)} \end{pmatrix} = \begin{pmatrix} \mathbf{f}^{(k)} \\ \bar{\mathbf{f}}^{(k)} \end{pmatrix}, \qquad 1 \le k \le K,$$

where $\mathcal{H}^{(0)}$ is given by (3.19) and $\mathbf{f}^{(k)}$ represents the right-hand side terms, which are defined recursively from the nonlinear Eq. (3.14). When $\boldsymbol{\phi}^{(k)} \in \omega \subset \Omega$, we have a unique solution of the inhomogeneous equations for any $1 \le k \le K$:

$$\phi_{n,m}^{(k)} = -\frac{1}{2} f_{n,m}^{(k)}, \quad (n, m) \in S_M, \qquad \phi_{n,m}^{(k)} = f_{n,m}^{(k)}, \qquad (n, m) \in \mathbb{Z}^2 \backslash S_M,$$

provided that

$$g_{n,m}^{(k)} = -\mathrm{Im}(f_{n,m}^{(k)} e^{-i\theta_{n,m}}) = 0, \qquad (n, m) \in S_M, \quad 1 \le k \le K.$$

Now, if all $\mathbf{g}^{(k)} = 0$ for $1 \le k \le K - 1$, but $(\mathbf{p}_1, \mathbf{g}^{(K)}) \ne 0$, where $\mathbf{p}_1$ is the derivative vector of (3.49) with respect to parameter θ, then the family (3.49) terminates at the Kth order of the Lyapunov–Schmidt reduction.

Following this algorithm, one can find that for $M = 1$, when $\mathbf{p}_1 = (0, 1, 0, 1)^T$, the vector $\mathbf{g}^{(k)}$ is zero for $k = 1, 2, 3, 4, 5$ and non-zero for $k = K = 6$. Moreover, $(\mathbf{p}_1, \mathbf{g}^{(6)}) \ne 0$ for any $\theta \ne \{0, \pi/2, \pi\}$. Similarly, in the case $M = 2$, we have also found that $K = 6$ and $(\mathbf{p}_1, \mathbf{g}^{(6)}) \ne 0$ for any $\theta \ne \{0, \pi/2, \pi\}$. Therefore, indeed, such solutions cannot be continued for the cases of $M = 1$ and 2. Finally, for $M = 3$, one obtains similar conclusions through numerical computations; it is therefore natural to conjecture that such a solution (asymmetric, one parameter family) cannot be continued to finite ϵ, for any value of M.

Summarizing our conclusions for the persistence of the different classified families of discrete solitons and discrete symmetric and asymmetric vortices, we have the following:

- discrete solitons of family (i) in (3.27)
- symmetric vortices of family (ii) in (3.28)
- asymmetric vortices of family (iii) in (3.29) cannot be continued to the domain $\epsilon \in \mathcal{O}(0)$ for $M = 1, 2, 3$.
- zero-parameter asymmetric vortices of family (iv) in (3.30)

It is now natural to turn to the examination of the stability of the relevant persisting solutions.

3.3.3 Stability of Discrete Solutions

To examine the spectral stability of discrete solitons and vortices, we use the linearization

$$u_{n,m}(t) = e^{i(1-4\epsilon)t}\left(\phi_{n,m} + a_{n,m}e^{\lambda t} + \bar{b}_{n,m}e^{\bar{\lambda}t}\right), \qquad (n,m) \in \mathbb{Z}^2, \tag{3.56}$$

where $\lambda \in \mathbb{C}$ and $(a_{n,m}, b_{n,m}) \in \mathbb{C}^2$ are the eigenvalues and eigenfunctions, respectively, satisfying

$$\begin{aligned} i\lambda a_{n,m} &= \left(1-2|\phi_{n,m}|^2\right)a_{n,m} - \phi_{n,m}^2 b_{n,m} \\ &\quad -\epsilon\left(a_{n+1,m} + a_{n-1,m} + a_{n,m+1} + a_{n,m-1}\right), \\ -i\lambda b_{n,m} &= -\bar{\phi}_{n,m}^2 a_{n,m} + \left(1-2|\phi_{n,m}|^2\right)b_{n,m} \\ &\quad -\epsilon\left(b_{n+1,m} + b_{n-1,m} + b_{n,m+1} + b_{n,m-1}\right). \end{aligned}$$

This stability problem can be rephrased as

$$i\lambda\boldsymbol{\psi} = \sigma\mathcal{H}\boldsymbol{\psi}, \tag{3.57}$$

where $\boldsymbol{\psi} = (a_{n,m}, b_{n,m})^T$ (the ^{T} denotes transpose), $\mathcal{H}$ is defined by the linearization operator (2.13), and σ consists of 2×2 blocks of Pauli matrices (σ_3 is the diagonal matrix with elements $(1,-1)$ along the diagonal). In the eigenvalue problem of Eq. (3.57), the presence of λ with non-zero real part illustrates the presence of instability.

The Taylor expansion of the matrix $\mathcal{H}$ will play a central role in our stability considerations below and is as follows:

$$\mathcal{H} = \mathcal{H}^{(0)} + \sum_{k=1}^{\infty}\epsilon^k\mathcal{H}^{(k)}, \tag{3.58}$$

where $\mathcal{H}^{(0)}$ is defined in (3.19), while the first- and second-order corrections are given by

$$\begin{aligned} \mathcal{H}_{n,m}^{(1)} = \; & -2\begin{pmatrix} \bar{\phi}_{n,m}^{(0)}\phi_{n,m}^{(1)} + \phi_{n,m}^{(0)}\bar{\phi}_{n,m}^{(1)} & \phi_{n,m}^{(0)}\phi_{n,m}^{(1)} \\ \bar{\phi}_{n,m}^{(0)}\bar{\phi}_{n,m}^{(1)} & \bar{\phi}_{n,m}^{(0)}\phi_{n,m}^{(1)} + \phi_{n,m}^{(0)}\bar{\phi}_{n,m}^{(1)} \end{pmatrix} \\ & -\left(s_{+1,0} + s_{-1,0} + s_{0,+1} + s_{0,-1}\right)\begin{pmatrix} 1 & 0 \\ 0 & 1 \end{pmatrix} \end{aligned}$$

and

$$\mathcal{H}_{n,m}^{(2)} = -2\begin{pmatrix} \bar{\phi}_{n,m}^{(0)}\phi_{n,m}^{(2)} + \phi_{n,m}^{(0)}\bar{\phi}_{n,m}^{(2)} & \phi_{n,m}^{(0)}\phi_{n,m}^{(2)} \\ \bar{\phi}_{n,m}^{(0)}\bar{\phi}_{n,m}^{(2)} & \bar{\phi}_{n,m}^{(0)}\phi_{n,m}^{(2)} + \phi_{n,m}^{(0)}\bar{\phi}_{n,m}^{(2)} \end{pmatrix} - \begin{pmatrix} 2|\phi_{n,m}^{(1)}|^2 & \phi_{n,m}^{(1)2} \\ \bar{\phi}_{n,m}^{(1)2} & 2|\phi_{n,m}^{(1)}|^2 \end{pmatrix}.$$

It is important to consider again the starting point of $\epsilon = 0$ and the eigenvalue count at that AC limit. There, $\mathcal{H}_{n,m} \equiv \mathcal{H}^{(0)}_{n,m}$ has exactly N negative eigenvalues $\gamma = -2$, N zero eigenvalues (these two sets will constitute the point spectrum of the solution with N excited sites), as well as infinitely many positive eigenvalues $\gamma = 1$ (these will become the continuous spectrum of the solution). In connection to the full eigenvalue problem of the stability operator $\sigma\mathcal{H}^{(0)}_{n,m}$, both the negative and zero eigenvalues correspond to $\lambda = 0$, while the $\gamma = 1$ positive eigenvalues correspond to $\lambda = \pm i$. As before in the one-dimensional problem (cf. Eqs. (2.34) and (2.35)), the latter part will develop a continuous spectral band $\lambda = \pm i[1 + 4\epsilon(\sin^2(q_n/2) + \sin^2(q_m/2))]$, extending in the interval $\pm i[1, 1 + 8\epsilon]$, which will be bounded away from the origin and will not produce instabilities for small ϵ. On the other hand, it is important to examine how the zero eigenvalues will move in the presence of the coupling-induced perturbation.

Focusing now on the zero eigenvalues of the operator $\mathcal{H}$ in the eigenvalue problem $\mathcal{H}\boldsymbol{\varphi} = \gamma\boldsymbol{\varphi}$, we can use the expansion

$$\boldsymbol{\varphi} = \boldsymbol{\varphi}^{(0)} + \epsilon\boldsymbol{\varphi}^{(1)} + \epsilon^2\boldsymbol{\varphi}^{(2)} + \mathrm{O}\left(\epsilon^3\right), \qquad \gamma = \epsilon\gamma_1 + \epsilon^2\gamma_2 + \mathrm{O}(\epsilon^3), \tag{3.59}$$

where $\boldsymbol{\varphi}^{(0)} = \sum_{j=1}^{N} c_j \mathbf{e}_j$ and $\mathbf{e}_j(\boldsymbol{\theta})$, $j = 1, \ldots, N$ are eigenvectors of the kernel of $\mathcal{H}^{(0)}$. These eigenvectors contain a single non-zero block $i(e^{i\theta_j}, -e^{-i\theta_j})^T$ at the jth position, which corresponds to the node (n, m) on the contour S_M and are orthogonal according to

$$(\mathbf{e}_i(\boldsymbol{\theta}), \mathbf{e}_j(\boldsymbol{\theta})) = 2\delta_{i,j}, \qquad 1 \le i, j \le N. \tag{3.60}$$

The corresponding generalized eigenvectors are $\hat{\mathbf{e}}_j(\boldsymbol{\theta})$, $j = 1, \ldots, N$, such that each eigenvector $\hat{\mathbf{e}}_j(\boldsymbol{\theta})$ contains the only non-zero block $(e^{i\theta_j}, e^{-i\theta_j})^T$ at the jth position. Direct computations show that

$$\sigma\mathcal{H}^{(0)}\hat{\mathbf{e}}_j(\boldsymbol{\theta}) = 2i\mathbf{e}_j(\boldsymbol{\theta}), \qquad 1 \le j \le N. \tag{3.61}$$

Then, the first-order correction in the eigenvalue equation for the matrix $\mathcal{H}$, $\boldsymbol{\varphi}^{(1)}$, satisfies the inhomogeneous equation

$$\mathcal{H}^{(0)}\boldsymbol{\varphi}^{(1)} + \mathcal{H}^{(1)}\boldsymbol{\varphi}^{(0)} = \gamma_1\boldsymbol{\varphi}^{(0)}. \tag{3.62}$$

Projection to the kernel of $\mathcal{H}^{(0)}$ gives the eigenvalue problem for γ_1:

$$\frac{1}{2}\sum_{i=1}^{N}\left(\mathbf{e}_j, \mathcal{H}^{(1)}\mathbf{e}_i\right)c_i = \gamma_1 c_j. \tag{3.63}$$

If one represents the operator $\mathcal{H}$ as $\mathcal{H} = \mathcal{H}_p + \epsilon\mathcal{H}_s$, then $\mathcal{H}^{(1)} = \mathcal{H}^{(1)}_p + \mathcal{H}_s$. On the other hand, the bifurcation conditions to leading order can be represented as

$$g_j^{(1)}(\boldsymbol{\theta}) = \frac{1}{2}\left(\mathbf{e}_j(\boldsymbol{\theta}), \mathcal{H}_s \boldsymbol{\phi}^{(0)}(\boldsymbol{\theta})\right).$$

A direct calculation then [14], of the left-hand side of Eq. (3.63) yields it to be equal to $\cos(\theta_j - \theta_{j+1}) + \cos(\theta_j - \theta_{j-1})$, which is also equal to the Jacobian element $(\mathcal{M}_1)_{ij} = \partial g_i^{(1)}/\partial \theta_j$. Hence for the N small eigenvalues of the eigenvalue problem $\mathcal{H}\boldsymbol{\varphi} = \gamma \boldsymbol{\varphi}$, we have

$$\lim_{\epsilon \to 0} \frac{\gamma_j}{\epsilon} = \mu_j^{(1)}, \qquad 1 \le j \le N, \tag{3.64}$$

where $\mu_j^{(1)}$ are the eigenvalues of $(\mathcal{M}_1)$.

It is then relevant to connect the eigenvalues of the Jacobian $\mathcal{M}_1$ (and of the matrix $\mathcal{H}$) to those of the full stability problem $\sigma \mathcal{H} \boldsymbol{\psi} = i\lambda \boldsymbol{\psi}$. The corresponding statement will be of the form

$$\lim_{\epsilon \to 0} \frac{\lambda_j^2}{\epsilon} = 2\mu_j^{(1)}, \qquad 1 \le j \le N. \tag{3.65}$$

This can be established by using the regular perturbation series

$$\boldsymbol{\psi} = \boldsymbol{\psi}^{(0)} + \sqrt{\epsilon}\boldsymbol{\psi}^{(1)} + \epsilon \boldsymbol{\psi}^{(2)} + \epsilon\sqrt{\epsilon}\boldsymbol{\psi}^{(3)} + \mathrm{O}(\epsilon^2), \tag{3.66}$$

$$\lambda = \sqrt{\epsilon}\lambda_1 + \epsilon\lambda_2 + \epsilon\sqrt{\epsilon}\lambda_3 + \mathrm{O}(\epsilon^2), \tag{3.67}$$

where, due to the relations (3.60) and (3.61), we have

$$\boldsymbol{\psi}^{(0)} = \sum_{j=1}^{N} c_j \mathbf{e}_j, \qquad \boldsymbol{\psi}^{(1)} = \frac{\lambda_1}{2} \sum_{j=1}^{N} c_j \hat{\mathbf{e}}_j, \tag{3.68}$$

according to the kernel and generalized kernel of $\sigma\mathcal{H}^{(0)}$. The second-order correction term $\boldsymbol{\psi}^{(2)}$ satisfies the inhomogeneous equation

$$\mathcal{H}^{(0)}\boldsymbol{\psi}^{(2)} + \mathcal{H}^{(1)}\boldsymbol{\psi}^{(0)} = i\lambda_1 \sigma \boldsymbol{\psi}^{(1)} + i\lambda_2 \sigma \boldsymbol{\psi}^{(0)}. \tag{3.69}$$

Projection to the kernel of $\mathcal{H}^{(0)}$ gives the eigenvalue problem for λ_1:

$$\mathcal{M}_1 \mathbf{c} = \frac{\lambda_1^2}{2}\mathbf{c}, \tag{3.70}$$

where $\mathbf{c} = (c_1, c_2, \ldots, c_N)^T$ and the matrix $\mathcal{M}_1$ is the same as in the eigenvalue problem (3.63). Relation (3.65) follows from (3.70).

Based on these results, we can quantify the number of eigenvalues of different types in the first-order reductions for the different families of solutions (except for the supersymmetric vortices that we will need to study at the second-order reduc-

tions since $\mathcal{M}_1 = 0$. In particular, considering the quantity A_1 defined in Eq. (3.36), we have that for the family (i), it is $A_1 = (-1)^{N-l}(2l - N)$, where l is the number of $+1$'s in the configuration. In that case $n(\mathcal{M}_1) = N - l - 1$, $z(\mathcal{M}_1) = 1$ and $p(\mathcal{M}_1) = l$ for $0 \leq l \leq 2M - 1$, while if $2M + 1 \leq l \leq 4M$, there is one more negative $(N - l)$ and one less positive $(l - 1)$ eigenvalue. In the supersymmetric case of $l = 2M$, $n(\mathcal{M}_1) = 2M - 1$, $z(\mathcal{M}_1) = 2$, and $p(\mathcal{M}_1) = 2M - 1$. This implies that for the number of real eigenvalue pairs N_r, imaginary ones with negative Krein signature N_i^-, and zero eigenvalues N_0, in this case we have $N_i^- = N - l - 1$, $N_0 = 1$, and $N_r = l$ for $0 \leq l \leq 2M - 1$; $N_i^- = N - l - 1$, $N_0 = 2$, and $N_r = l - 1$ for $l = 2M$; and $N_i^- = N - l$, $N_0 = 1$, and $N_r = l - 1$ for $2M + 1 \leq l \leq N$.

In the case of family (ii), the corresponding counts for $\mathcal{M}_1$ are $n(\mathcal{M}_1) = 0$, $z(\mathcal{M}_1) = 1$, and $p(\mathcal{M}_1) = N - 1$ for $1 \leq L \leq M - 1$ and $n(\mathcal{M}_1) = N - 1$, $z(\mathcal{M}_1) = 1$, and $p(\mathcal{M}_1) = 0$ for $M + 1 \leq L \leq 2M - 1$, for discrete vortices of charge L within the contour S_M. This, in turn, implies that the full eigenvalue problem will have $N_i^- = 0$, $N_0 = 1$, and $N_r = N - 1$ for $1 \leq L \leq M - 1$; $N_i^- = 0$, $N_0 = N$, and $N_r = 0$ for $L = M$; and $N_i^- = N - 1$, $N_0 = 1$, and $N_r = 0$ for $M + 1 \leq L \leq 2M - 1$.

Having eliminated the potential for the monoparametric asymmetric vortices of family (iii), we lastly examine the zero parameter asymmetric vortices of family (iv) in the realm of first-order reductions. We find there for $\cos\theta_* \neq 0$, $L \neq M$ and $1 \leq n \leq N - 1$, $n \neq 2M$, that the parameter $A_1 = (-1)^{N-n}(\cos\theta_*)^{N-1}(2n - N)$, such that $z(\mathcal{M}_1) = 1$ in all cases. For $\cos\theta_* > 0$, $n(\mathcal{M}_1) = N - n - 1$ and $p(\mathcal{M}_1) = n$ for $1 \leq n \leq 2M - 1$ and $n(\mathcal{M}_1) = N - n$ and $p(\mathcal{M}_1) = n - 1$ for $2M + 1 \leq n \leq N - 1$. In the opposite case of $\cos\theta_* < 0$, we have $n(\mathcal{M}_1) = n$ and $p(\mathcal{M}_1) = N - n - 1$ for $1 \leq n \leq 2M - 1$ and $n(\mathcal{M}_1) = n - 1$ and $p(\mathcal{M}_1) = N - n$ for $2M + 1 \leq n \leq N - 1$. These results lead to the full eigenvalue problem counts: for $\cos\theta_* > 0$, we have $N_i^- = N - n - 1$, $N_0 = 1$, and $N_r = n$ for $1 \leq n \leq 2M - 1$ and $N_i^- = N - n$, $N_0 = 1$, and $N_r = n - 1$ for $2M + 1 \leq n \leq N - 1$; for $\cos\theta_* < 0$, we have $N_i^- = n$, $N_0 = 1$, and $N_r = N - n - 1$ for $1 \leq n \leq 2M - 1$ and $N_i^- = n - 1$, $N_0 = 1$, and $N_r = N - n$ for $2M + 1 \leq n \leq N - 1$.

Despite the considerable wealth of information provided by the first-order reductions, there are still features that need to be clarified at the second-order reductions. Among them are the second zero eigenvalue of supersymmetric solitons (that should bifurcate away from the origin at a higher order), the potential splitting of real eigenvalues of the first-order reductions in the complex plane for solutions of family (ii), or the analysis of the stability of supersymmetric vortices with $L = M$ within family (ii).

3.3.3.1 Eigenvalue Splitting at Second-Order Reductions

In the case of family (i), for $l = 2M$ (supersymmetric solitons) and $a_j \neq (-1)^j a$, as indicated above the Jacobian has two zero eigenvalues with eigenvectors $\mathbf{p}_0$ and $\mathbf{p}_1$. On the other hand, the matrix $\mathcal{M}_1 + \epsilon\mathcal{M}_2$ has only one zero eigenvalue with eigenvector $\mathbf{p}_0$ (due to the gauge invariance). Therefore, the second eigenvalues should bifurcate away from zero at the second-order reduction. We can therefore expand

the perturbation theory at the next order using $\mathbf{c} = \mathbf{p}_1$ to derive

$$\gamma_2 = \frac{(\mathbf{p}_1, \mathcal{M}_2 \mathbf{p}_1)}{(\mathbf{p}_1, \mathbf{p}_1)}.$$

One can therefore find at the second order that

$$\lambda_2^2 = 2\frac{(\mathbf{p}_1, \mathcal{M}_2 \mathbf{p}_1)}{(\mathbf{p}_1, \mathbf{p}_1)} = 2\gamma_2.$$

It can therefore be concluded that the splitting of the additional zero eigenvalue in the second-order reduction resembles that of the zero eigenvalues in the first-order reductions. If $\gamma_2 > 0$, then the eigenvalues $\epsilon\lambda_2$ will be real, while if $\gamma_2 < 0$, they will be imaginary with negative Krein sign.

The next topic of interest that needs to be addressed at the level of second-order reductions is the potential splitting of non-zero eigenvalues (of the first order). In particular, if we use the explicit solutions for $\boldsymbol{\phi}^{(1)}$, required in $\mathcal{H}^{(1)}$, it is possible to compute the explicit solution of the inhomogeneous equation (3.69) for $\boldsymbol{\psi}^{(2)}$ as

$$\begin{aligned}\boldsymbol{\psi}^{(2)} = &\frac{\lambda_2}{2}\sum_{j=1}^{N} c_j \hat{\mathbf{e}}_j + \frac{1}{2}\sum_{j=1}^{N}(\sin(\theta_{j+1}-\theta_j)c_{j+1} + \sin(\theta_{j-1}-\theta_j)c_{j-1})\hat{\mathbf{e}}_j \\ &+ \sum_{j=1}^{N} c_j\left(\mathcal{S}_+ + \mathcal{S}_-\right)\mathbf{e}_j,\end{aligned} \tag{3.71}$$

where the operators $\mathcal{S}_\pm$ shift elements of $\mathbf{e}_j$ from the node $(n, m) \in S_M$ to the adjacent nodes outside of S_M. Then, for the third-order correction $\boldsymbol{\psi}^{(3)}$, one has the subsequent order inhomogeneous equation of the form

$$\mathcal{H}^{(0)}\boldsymbol{\psi}^{(3)} + \mathcal{H}^{(1)}\boldsymbol{\psi}^{(1)} = i\lambda_1\sigma\boldsymbol{\psi}^{(2)} + i\lambda_2\sigma\boldsymbol{\psi}^{(1)} + i\lambda_3\sigma\boldsymbol{\psi}^{(0)}. \tag{3.72}$$

To obtain an expression for the second-order correction λ_2, we project the inhomogeneous problem (3.72) also to the kernel of $\mathcal{H}^{(0)}$ (as before to obtain Eq. (3.70)), which, in turn, leads to

$$\mathcal{M}_1\mathbf{c} = \frac{\lambda_1^2}{2}\mathbf{c} + \sqrt{\epsilon}\left(\lambda_1\lambda_2\mathbf{c} + \lambda_1\mathcal{L}_1\mathbf{c}\right), \tag{3.73}$$

where the matrix $\mathcal{L}_1$ is defined by

$$(\mathcal{L}_1)_{i,j} = \begin{cases}\sin(\theta_j - \theta_i), & i = j \pm 1, \\ 0, & |i-j| \neq 1,\end{cases} \tag{3.74}$$

subject to the periodic boundary conditions. If we now label the eigenvalue of the first-order Jacobian matrix $\mathcal{M}_1$ as $\mu_j^{(1)}$ (with eigenvector $\mathbf{c}_j$), then the two leading

order expressions for the bifurcation of the eigenvalue from zero in Eq. (3.66) are given by

$$\lambda_1 = \pm\sqrt{2\mu_j^{(1)}}, \qquad \lambda_2 = -\frac{(\mathbf{c}_j, \mathcal{L}_1\mathbf{c}_j)}{(\mathbf{c}_j, \mathbf{c}_j)}. \tag{3.75}$$

Now, given the skew-symmetric nature of the operator $\mathcal{L}_1$, we infer that the second-order correction term λ_2 is purely imaginary or zero. In the case of discrete solitons of family (i), since $\sin(\theta_{j+1}-\theta_j) = 0$, the elements of $\mathcal{L}_1$ (and hence λ_2) will be vanishing. On the other hand, in the case of symmetric vortices of family (ii) with $L \neq M$, the matrix $\mathcal{M}_1$ has double eigenvalues, according to the roots of $\sin^2 \pi n/N$ in the explicit solution (3.37). In that case, all the coefficients $a_j = \cos(\theta_{j+1} - \theta_j)$ and $b_j = \sin(\theta_{j+1} - \theta_j)$, $1 \leq j \leq N$ will be the same: $a_j = a$ and $b_j = b$. Then, one can again compute both the first, as well as the second-order correction for the eigenvalues explicitly as

$$\lambda_1 = \pm\sqrt{8a}\sin\frac{\pi n}{N}, \quad \lambda_2 = -2ib\sin\frac{2\pi n}{N}, \quad 1 \leq n \leq N. \tag{3.76}$$

This implies that all double roots of λ_1 with $n \neq N/2$ and N split along the imaginary axis in λ_2. When $a > 0$, the splitting occurs in the transverse directions to the real values of λ_1. When $a < 0$, the splitting occurs in the longitudinal directions to the imaginary values of λ_1. The simple roots at $n = N/2$ and N are not affected, since $\lambda_2 = 0$ for $n = N/2$ and N. This implies, e.g., that for discrete vortices of family (ii) with $1 \leq L \leq M - 1$, their positive double roots will, in fact, split and become into complex quartets, as we will see below for example in the case of $M = 2$ and $L = 1$.

We now turn to the case of supersymmetric vortices (where the first-order reductions are completely degenerate and yield no information) in order to use the second-order reductions to address the splitting of their zero eigenvalues. We extend the results of the regular perturbation series (3.59) and (3.66) to the case $\mathcal{M}_1 = 0$, which occurs for supersymmetric vortices of family (ii) with charge $L = M$. More specifically, when $\mathcal{M}_1 = 0$ (and hence $\gamma_1 = 0$), then the first-order correction is given by

$$\boldsymbol{\varphi}^{(1)} = \frac{1}{2}\sum_{j=1}^{N}(c_{j+1} - c_{j-1})\hat{\mathbf{e}}_j + \sum_{j=1}^{N} c_j\,(\mathcal{S}_+ + \mathcal{S}_-)\,\mathbf{e}_j, \tag{3.77}$$

where the meaning of the operators $\mathcal{S}_\pm$ is the same as in Eq. (3.71). Going to the next order in perturbation theory, we obtain the inhomogeneous equation

$$\mathcal{H}^{(0)}\boldsymbol{\varphi}^{(2)} + \mathcal{H}^{(1)}\boldsymbol{\varphi}^{(1)} + \mathcal{H}^{(2)}\boldsymbol{\varphi}^{(0)} = \gamma_2\boldsymbol{\varphi}^{(0)}. \tag{3.78}$$

Hence, projecting to the kernel of $\mathcal{H}^{(0)}$ gives the eigenvalue problem for γ_2:

$$\frac{1}{2}\left(\mathbf{e}_j, \mathcal{H}^{(1)}\boldsymbol{\varphi}^{(1)}\right) + \frac{1}{2}\sum_{i=1}^{N}\left(\mathbf{e}_j, \mathcal{H}^{(2)}\mathbf{e}_i\right)c_i = \gamma_2 c_j. \tag{3.79}$$

Through direct computation, one can verify that the matrix on the left-hand side of (3.79) is identical to the Jacobian matrix $\mathcal{M}_2$ (defined as $(\mathcal{M}_2)_{ij} = \partial \mathbf{g}_i^{(2)}/\partial\theta_j$). Using our results from the Jacobian of the second-order reductions in the previous section (for $M = 1$, 2, and 3), we have that $n(\mathcal{M}_2) = 0$, $z(\mathcal{M}_2) = 2$, and $p(\mathcal{M}_2) = 2$ for $M = 1$; $n(\mathcal{M}_2) = 1$, $z(\mathcal{M}_2) = 2$, and $p(\mathcal{M}_2) = 5$ for $M = 2$; and $n(\mathcal{M}_2) = 4$, $z(\mathcal{M}_2) = 2$, and $p(\mathcal{M}_2) = 6$ for $M = 3$. We now need to connect the eigenvalues of the Jacobian matrix $\mathcal{M}_2$ with those of the full eigenvalue problem λ, This is done again by using the perturbation series but now in the form

$$\boldsymbol{\psi} = \boldsymbol{\psi}^{(0)} + \epsilon\boldsymbol{\psi}^{(1)} + \epsilon^2\boldsymbol{\psi}^{(2)} + \mathrm{O}(\epsilon^3), \qquad \lambda = \epsilon\lambda_1 + \epsilon^2\lambda_2 + \mathrm{O}(\epsilon^3), \tag{3.80}$$

where

$$\boldsymbol{\psi}^{(0)} = \sum_{j=1}^{N} c_j\mathbf{e}_j, \qquad \boldsymbol{\psi}^{(1)} = \boldsymbol{\varphi}^{(1)} + \frac{\lambda_1}{2}\sum_{j=1}^{N} c_j\hat{\mathbf{e}}_j, \tag{3.81}$$

and $\boldsymbol{\varphi}^{(1)}$ is given by (3.77). The second-order correction term $\boldsymbol{\psi}^{(2)}$ is found from the inhomogeneous equation

$$\mathcal{H}^{(0)}\boldsymbol{\psi}^{(2)} + \mathcal{H}^{(1)}\boldsymbol{\psi}^{(1)} + \mathcal{H}^{(2)}\boldsymbol{\psi}^{(0)} = i\lambda_1\sigma\boldsymbol{\psi}^{(1)} + i\lambda_2\sigma\boldsymbol{\psi}^{(0)}. \tag{3.82}$$

In this case, the projection of the inhomogeneous equation to the kernel of $\mathcal{H}^{(0)}$ gives the eigenvalue problem for λ_1:

$$\mathcal{M}_2\mathbf{c} = \lambda_1\mathcal{L}_2\mathbf{c} + \frac{\lambda_1^2}{2}\mathbf{c}, \tag{3.83}$$

where $\mathbf{c} = (c_1, c_2, \ldots, c_N)^T$, the matrix $\mathcal{M}_2$ is the same as in the eigenvalue problem (3.79), and the matrix $\mathcal{L}_2$ follows from the matrix $\mathcal{L}_1$ in the form (3.74) with $\sin(\theta_{j+1} - \theta_j) = 1$, or explicitly:

$$(\mathcal{L}_2)_{i,j} = \begin{cases} +1, & i = j - 1, \\ -1, & i = j + 1, \\ 0, & |i - j| \neq 1, \end{cases} \tag{3.84}$$

subject to the periodic boundary conditions. Given that $\mathcal{M}_2$ is symmetric and $\mathcal{L}_2$ is skew-symmetric, the eigenvalues of the problem (3.83) arise in pairs $(\lambda_1, -\lambda_1)$. A direct comparison of the matrices $\mathcal{M}_2$ in (3.50) and $\mathcal{L}_2$ in (3.84), leads to the conclusion $\mathcal{M}_2 = -(1/2)\mathcal{L}_2^2$. However, the Jacobian matrices $\tilde{\mathcal{M}}_2$ are modified in the case $M = 2$ and $M \geq 3$ by the rank-one and rank-four non-positive matrices $\Delta\mathcal{M}_2$. As a result, the eigenvalue problem (3.83) can be factorized as follows:

$$\frac{1}{2}\left(\mathcal{L}_2+\lambda_1\right)^2\mathbf{c}=\Delta\mathcal{M}_2\mathbf{c}. \tag{3.85}$$

One can now consider the reduced eigenvalue problem of Eq. (3.83) in the cases of $M=1$, 2, and 3. In the case of $M=1$, the problem takes the form of the following constant-coefficient difference equation:

$$-c_{j+2}+2c_j-c_{j-2}=\lambda_1^2c_j+2\lambda_1\left(c_{j+1}-c_{j-1}\right),\qquad 1\le j\le 4M, \tag{3.86}$$

subject to the periodic boundary conditions, which, as usual, can be tackled by the discrete Fourier transform yielding

$$\left(\lambda_1+2i\sin\frac{\pi n}{2M}\right)^2=0,\qquad 1\le n\le 4M. \tag{3.87}$$

This implies that the eigenvalue problem will have two eigenvalue pairs with $\lambda_1=\pm 2i$, and two more pairs of eigenvalues with $\lambda_1=0$ (only one of which will persist to higher order reductions).

On the other hand, in the case of $M=2$, the problem of Eq. (3.83) can be reduced to two constant-coefficient difference equations

$$\begin{aligned}
&-x_{j+1}+2x_j-x_{j-1}=\lambda_1^2x_j+2\lambda_1\left(y_j-y_{j-1}\right),\quad j=1,2,3,4,\\
&y_{j+1}-2y_{j+2}+y_{j-1}=\lambda_1^2y_j+2\lambda_1\left(x_{j+1}-x_j\right),\quad j=1,2,3,4,
\end{aligned}$$

where $x_j=c_{2j-1}$ and $y_j=c_{2j}$ are subject to the periodic boundary conditions. In this case, the characteristic equation has the explicit form

$$\lambda_1^4-2\lambda_1^2\left(1-(-1)^n-8\sin^2\frac{\pi n}{4}\right)+8\sin^2\frac{\pi n}{4}\left(1-(-1)^n-2\sin^2\frac{\pi n}{4}\right)=0$$

for $n=1,2,3,4$, leading to four pairs of eigenvalues with $\lambda_1=\pm\sqrt{2}i$, a single pair with $\lambda_1=\pm\sqrt{\sqrt{80}-8}$ (which renders the configuration with $L=M=2$ *immediately* unstable for $\epsilon\neq 0$), a single pair with $\lambda_1=\pm i\sqrt{\sqrt{80}+8}$ and finally two pairs with $\lambda_1=0$, only one of which will survive for higher order reductions.

Finally, in the case of $M=3$, it is less straightforward to compute the eigenvalues explicitly via Fourier decomposition. For this reason, we instead obtain them from a numerical linear algebra package as

$$\begin{aligned}
&\lambda_{1,2}=\pm 3.68497i,\quad \lambda_{3,4}=\lambda_{5,6}=\pm 3.20804i,\quad \lambda_{7,8}=\pm 2.25068i,\\
&\lambda_{9,10}=\lambda_{11,12}=\pm i,\ \lambda_{13,14}=\lambda_{15,16}=\pm 0.53991,\\
&\lambda_{17,18,19,20}=\pm 0.634263\pm 0.282851i,\quad \lambda_{21,22,23,24}=0.
\end{aligned}$$

Therefore, in the case of the $L=M=3$, we expect a double real eigenvalue pair and a complex eigenvalue quartet to immediately destabilize the relevant

configuration (although additional potentially unstable eigendirections may exist, since the algebraic multiplicity of the zero eigenvalue is larger than two).

It is interesting to slightly expand here on the reasons for the destabilization of the $L = M = 2$ and $L = M = 3$ supersymmetric vortex solutions. More specifically, the destabilization of the supersymmetric vortex with $M = 2$ occurs due to the center node $(2, 2)$, which couples its nearest-neighbors of the contour S_2 in the second-order reductions. This modifies the Jacobian matrix $\tilde{\mathcal{M}}_2$ (due to the non-zero nature of the rank-one non-positive matrix $\Delta\mathcal{M}_2$) in a way such as to produce a simple negative eigenvalue, while none such exists for the non-negative matrix $\mathcal{M}_2$. A similar feature arises in the destabilization of the $L = M = 3$ supersymmetric vortex, whereby the coupling of eight nodes of the contour S_3 with four interior corner points $(2, 2)$, $(2, M)$, (M, M), and $(M, 2)$ induces the destabilization. In the latter case, the rank-four non-positive matrix $\Delta\mathcal{M}_2$ leads to four negative eigenvalues in the Jacobian matrix $\tilde{\mathcal{M}}_2$ and to four unstable eigenvalues in the reduced eigenvalue problem (3.85). It is interesting that this mathematical quantification leads to an intuitive understanding of the origin of the instability and, therefore, to insights as to how to avoid it. In particular, the latter can be achieved, for instance, if a hole is drilled at the central node (2,2) of the $M = 2$ contour, or four such holes at the sites $(2, 2)$, $(2, M)$, (M, M), and $(M, 2)$ of the $M = 3$ contour, then the matrix $\Delta\mathcal{M}_2 = 0$; then, all the relevant eigenvalues of the Jacobian would be positive leading to imaginary eigenvalues for the full eigenvalue problem, similarly to the case of $M = 1$. We will test this type of insight numerically in what follows.

3.3.3.2 Eigenvalue Splitting at Higher Order Reductions

It is important to note that in all the above supersymmetric cases, there are additional (to the ones stemming from the gauge invariance) zero eigenvalues at the level of the second-order corrections, which need to be resolved at the level of higher order reductions. In particular, we consider the splitting of the double zero eigenvalue of $\mathcal{M}_2$ which corresponds to the eigenvectors $\mathbf{p}_0$ and $\mathbf{p}_1$, where $\mathbf{p}_0 = (1, 1, \ldots, 1, 1)^T$ and $\mathbf{p}_1 = (0, 1, \ldots, 0, 1)^T$. To this effect, we set $\mathbf{c} = (c_1, \ldots, c_N) = \mathbf{p}_1 + \alpha\mathbf{p}_0$, where α is a parameter and generally assume that the splitting occurs at the Kth order of reductions. Then, the perturbation series (3.59) needs to be extended to that order, leading to the following inhomogeneous equation:

$$\mathcal{H}^{(0)}\boldsymbol{\varphi}^{(k)} = -\sum_{m=1}^{k} \mathcal{H}^{(m)}\boldsymbol{\varphi}^{(k-m)}, \qquad 1 \le k \le K-1$$

and

$$\mathcal{H}^{(0)}\boldsymbol{\varphi}^{(K)} = -\sum_{m=1}^{K} \mathcal{H}^{(m)}\boldsymbol{\varphi}^{(K-m)} + \gamma_K\boldsymbol{\varphi}^{(0)},$$

where the zeroth order $\boldsymbol{\varphi}^{(0)} = \sum_{j=1}^{N} c_j\mathbf{e}_j$, and $\gamma = \gamma_K\epsilon^K + \mathrm{O}(\epsilon^{K+1})$ is the leading order approximation for the smallest non-zero eigenvalue of $\mathcal{H}$. From the projection

formulas on to the kernel of $\mathcal{H}^{(0)}$, then the equations for the correction γ_K and α can be obtained.

This algorithmic procedure can be used for the supersymmetric vortices with $M = 1$, leading to $K = 6$, $\alpha = -1/2$, and $\gamma_6 = -16$ (and, hence, to the conclusion that the zero eigenvalue becomes a small negative eigenvalue for small $\epsilon \neq 0$). A similar conclusion is obtained for $M = 2$, where $K = 6$, $\alpha = -1/2$, and $\gamma_6 = -8$. This allows us to develop the regular perturbation series for the eigenvalue problem $\sigma\mathcal{H}\boldsymbol{\psi} = i\lambda\boldsymbol{\psi}$ starting with the zeroth order $\boldsymbol{\psi}^{(0)} = \sum_{j=1}^{N} c_j \mathbf{e}_j$ and $\mathbf{c} = \mathbf{p}_1 + \alpha\mathbf{p}_0$, where $\alpha = -1/2$. This leads in the case of $M = 1$ to the conclusion that $\lambda_1 = \lambda_2 = 0$ but $\lambda_3 \neq 0$, such that $\lambda_3^2 = -32 = 2\gamma_6$; this results in a small imaginary eigenvalue of the linear stability matrix with negative Krein signature. Similarly, for the case of $M = 2$, we find that $\lambda_3^2 = -16 = 2\gamma_6$.

Based on the above results, we can summarize our stability conclusions as follows. We expect in the vicinity of $\epsilon \in \mathcal{O}(0)$ to have stable solutions of the following forms:

- discrete solitons,
- discrete symmetric vortices of family (ii) over contours S_M with charge $M + 1 \leq L \leq 2M - 1$,
- discrete supersymmetric vortices with $L = M = 1$.

We now turn to a numerical examination of the above findings.

3.3.4 Numerical Results

3.3.4.1 Discrete Solitons

Based on the above considerations, we can firstly construct any discrete soliton configuration that we would like (comprising essentially of $+1$'s and -1's on the lattice) at the AC limit. We can subsequently continue the relevant configuration to finite values of the coupling ϵ, by solving Eq. (3.6) and finally obtain the corresponding linearization eigenvalues, by solving the linear stability problem $\sigma\mathcal{H}\boldsymbol{\psi} = i\lambda\boldsymbol{\psi}$ numerically.

For the case of discrete solitons, we will only consider some illustrative cases to highlight the comparison of theoretical and numerical results, although it should be stressed that the same approach can essentially be used for any configuration of interest. Any two-site configuration in the two-dimensional problem can be effectively thought of as a quasi-one-dimensional one along the line of sight connecting the two sites. Keep in mind, however, that this is genuinely true only when the sites are connected by a lattice direction; when they are not, the relevant eigenvalues are expected to be non-zero to leading order at $\epsilon^{d_{min}/2}$ where d_{min} is the minimal distance between the sites along the lattice directions. Hence, to consider genuinely non-quasi-one-dimensional properties, we need to examine configurations with three or more sites. As a prototypical three-site example, we will consider the following configuration:

$$\begin{pmatrix} 1 & 0 & -1 \\ 0 & 0 & 0 \\ 0 & 0 & 1 \end{pmatrix}. \tag{3.88}$$

We will also consider two prototypical four site configurations, namely

$$\begin{pmatrix} 1 & 0 & -1 \\ 0 & 0 & 0 \\ -1 & 0 & 1 \end{pmatrix} \text{ and } \begin{pmatrix} 1 & -1 & -1 \\ 0 & 1 & 0 \\ 0 & 0 & 0 \end{pmatrix}, \tag{3.89}$$

as well as two five-site configurations

$$\begin{pmatrix} 1 & 0 & 1 \\ 0 & -1 & 0 \\ 1 & 0 & 1 \end{pmatrix} \text{ and } \begin{pmatrix} 0 & -1 & 1 \\ 0 & 1 & 0 \\ 1 & -1 & 0 \end{pmatrix}. \tag{3.90}$$

The above matrices yield the spatial form of the (real) field at the anti-continuum limit, in the vicinity of the spatially excited sites. For completeness/comparison, we also consider a configuration with many more sites such as the nine-site configuration of the form

$$\begin{pmatrix} 1 & -1 & 1 \\ -1 & 1 & -1 \\ 1 & -1 & 1 \end{pmatrix}. \tag{3.91}$$

For the three-site configuration, for bifurcation equation purposes, the structure is similar to the three-site one-dimensional structures of Fig. 2.12 of the previous chapter. Hence, the relevant Jacobian and eigenvalues in this case also will be $\lambda = \pm\sqrt{2}\epsilon$ and $\pm\sqrt{6}\epsilon$ (in addition to the zero eigenvalue of the phase invariance); see the relevant discussion around Eq. (2.86).

For the four-site configurations of (3.89), as regards the first configuration, the bifurcation equations for all four sites are $g_j = \sin(\theta_j - \theta_{j+1}) + \sin(\theta_j - \theta_{j-1})$, where θ_j is the phase (0 or π depending on whether the AC limit is $+1$ or -1 for each site) and $\theta_{j\pm1}$ is the phase of their closest two neighbors in the configuration. From this, once again the first-order reduction Jacobian can be computed, leading to the eigenvalues $\lambda = \pm 2\epsilon i$ (a double eigenvalue pair) and $\lambda = \pm 2\sqrt{2}\epsilon i$ (a single pair) in addition to the zero eigenvalue of the phase invariance. For the second four-site configuration of (3.89), the bifurcation equations are slightly more complicated in that the site that has three neighbors has $g_2 = \sin(\theta_2 - \theta_1) + \sin(\theta_2 - \theta_3) + \sin(\theta_2 - \theta_4)$, where θ_2 is the phase of that site and $\theta_{1,3,4}$ those of its neighbors, while the rest of the sites have $g_j = \sin(\theta_j - \theta_2)$ for $j = 1, 3, 4$. From the corresponding Jacobian one can extract the relevant eigenvalues to be $\lambda = \pm\sqrt{2\epsilon}i$ (a double eigenvalue) and $\lambda = \pm\sqrt{8\epsilon}i$ (a single eigenvalue), as well as the zero eigenvalue pair.

For the first five-site configurations of (3.90), we have the bifurcation equation $g_0 = 2\sin(\theta_0 - \theta_1) + 2\sin(\theta_0 - \theta_2) + 2\sin(\theta_0 - \theta_3) + 2\sin(\theta_0 - \theta_4)$, where we

have labeled as θ_0 the phase of the central site, while θ_j, with $j = 1, 2, 3, 4$, denote the phases of the four corner sites. We also have for the corner sites $g_j = \sin(\theta_j - \theta_{j+1}) + \sin(\theta_j - \theta_{j-1}) + 2\sin(\theta_j - \theta_0)$ for $j = 1, 2, 3, 4$. In this case, in addition to the zero eigenvalue, there is a real eigenvalue pair $\lambda = \pm 2\epsilon$, an eigenvalue of $\mathcal{O}(\epsilon^2)$ and an imaginary pair $\lambda = \pm\sqrt{20}\epsilon i$. Hence, this configuration is predicted to *always* be linearly unstable. Finally, for the second five-site configuration, one can similarly write down the bifurcation equations and accordingly obtain the eigenvalues: $\lambda = \pm 0.874 i\sqrt{\epsilon}$, $\pm 1.6625 i\sqrt{\epsilon}$, $\pm 2.288 i\sqrt{\epsilon}$, and $\pm 2.69 i\sqrt{\epsilon}$, as well as the zero eigenvalue.

Finally, for the configuration with nine sites of (3.91), labeling θ_0 the phase of the central site of the contour, $\theta_{1,3,5,7}$ the phases of the four corners, and $\theta_{2,4,6,8}$ those of the four sites adjacent to the central one, we have the bifurcation equations $g_j = \sin(\theta_j - \theta_{j+1}) + \sin(\theta_j - \theta_{j-1})$ for $j = 1, 3, 5, 7$, while $g_j = \sin(\theta_j - \theta_{j+1}) + \sin(\theta_j - \theta_{j-1}) + \sin(\theta_j - \theta_0)$ for $j = 2, 4, 6, 8$, and $g_0 = \sum_{k=1}^{4} \sin(\theta_0 - \theta_{2k})$. From the corresponding Jacobian the first-order reduction for the eigenvalues yields $\lambda = \pm\sqrt{2\epsilon}i$ (double), $\lambda = \pm 2\sqrt{\epsilon}i$ (single), $\lambda = \pm\sqrt{6\epsilon}i$ (double), $\lambda = \pm\sqrt{8\epsilon}i$ (double), and $\lambda = \pm\sqrt{12\epsilon}i$ (single), with the parenthesis denoting in each case the multiplicity of the relevant eigenvalue.

The results for the three-site configuration of (3.88) are shown in Fig. 3.3. We illustrate the configuration for two different values of the coupling (one stable and one unstable, while the comparison of the theoretically predicted and numerically obtained eigenvalues is shown in the bottom panel. It can be seen that the agreement is very good between the two. The configuration is, in fact, found to be unstable for $\epsilon > 0.295$, when the larger of the two imaginary eigenvalues of negative Krein sign collides with an eigenvalue bifurcating from the lower band edge of the continuous spectrum, leading to an oscillatory instability through the generation of a quartet of eigenvalues.

Figure 3.4 shows the two cases of (3.89) concerning four-site solutions. The top left panel shows the first configuration which is linearly stable for small values of

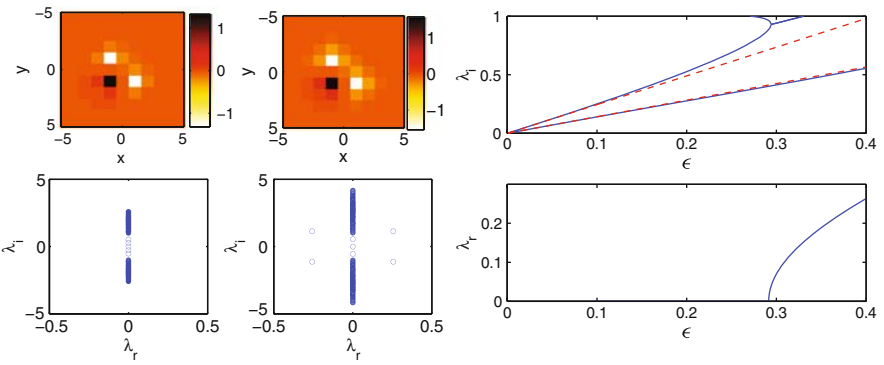

Fig. 3.3 The *left two rows* show the three-site solution of (3.88) for $\epsilon = 0.2$ and 0.4 and the corresponding linear stability eigenvalues (the former case is stable, while the latter is unstable). The *right row* shows the evolution of the imaginary (*top*) and real (*bottom*) eigenvalues as a function of ϵ. The *solid lines* show the full numerical results, while the dashed lines indicate the corresponding theoretical predictions

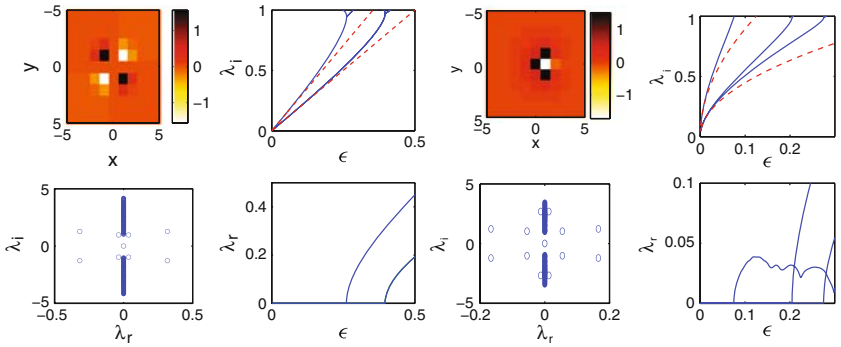

Fig. 3.4 The *four left panels* concern the first solution of (3.89), while the *four right panels* concern the second one. The *top left panel* in each case shows a typical solution profile (for $\epsilon = 0.4$ in the *left rows*, and for $\epsilon = 0.3$ in the *right rows*), the *bottom left* the corresponding eigenvalues in the spectral plane, while the *top* and *bottom right* in each case show the dependence on ϵ of the imaginary and real parts of the relevant eigenvalues (again the *solid lines* correspond to the numerical results, while *dashed* ones to theoretical approximations discussed above)

ϵ, with a double and a single imaginary eigenvalue pairs with negative Krein sign. These eigenvalues eventually destabilize the solution upon collision with eigenvalues bifurcating from the band edge of the continuous spectrum. The relevant collisions occur for $\epsilon = 0.262$ and 0.396. The right panels show the second configuration whose three imaginary negative Krein sign eigenvalues collide with the band edge at $\epsilon = 0.076$, 0.206, and 0.276 giving rise to three eigenvalue quartets.

The five-site configurations of (3.90) are, in turn, shown in Fig. 3.5. Note that the first one of these configurations is immediately unstable, as soon as $\epsilon \neq 0$, due to a very accurately captured real eigenvalue pair $\lambda = \pm 2\epsilon$. Additionally, there is complex quartet emerging from the collision of the $\mathcal{O}(\epsilon)$ imaginary eigenvalue of

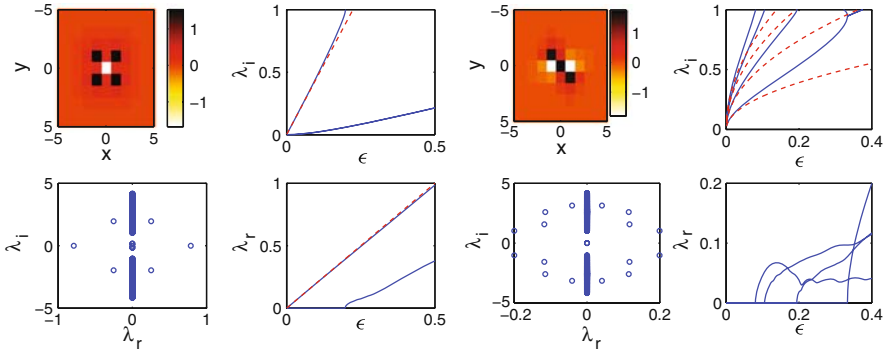

Fig. 3.5 Same as Fig. 3.4, but now for the five-site configurations of (3.90). The four left panels correspond to the first configuration, while the right four panels to the second configuration. Note the immediate instability of the former. The numerical solutions and their linear stability are for $\epsilon = 0.4$

the configuration with the continuous spectrum at $\epsilon = 0.198$. On the other hand, the double pair of $\mathcal{O}(\epsilon^2)$ eigenvalues moves more slowly and does not collide with the band edge for the parameter values considered. On the other hand, the second configuration is stable for small ϵ, but becomes increasingly unstable as ϵ is increased due to a sequence of four collisions with the band edge (or eigenvalues bifurcating from the band edge) of the continuous spectrum occurring at $\epsilon = 0.081$, 0.106, 0.195, and $\epsilon = 0.334$.

Finally, the nine-site waveform of (3.91) is demonstrated in Fig. 3.6, along with the dependence of its eigenvalues on ϵ. Once again as predicted by the theory, the solution is found to be linearly stable with eight imaginary eigenvalue pairs (three of which are double) for small ϵ. However, for $\epsilon > 0.054$, a complex web of oscillatory instabilities is initiated (which is also affected by finite size effects in the figure, discussed in more detail in the chapter on dark solitons), rendering the solution unstable thereafter.

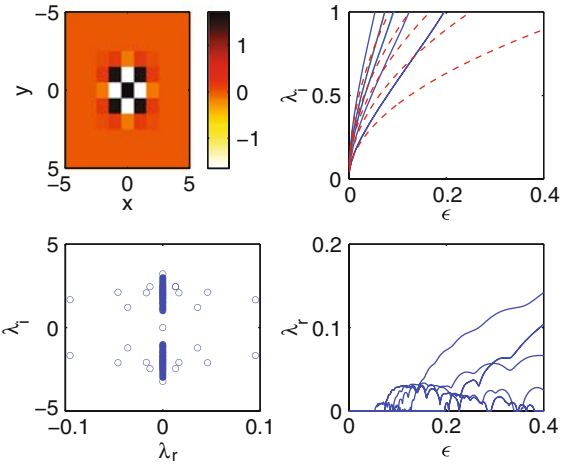

Fig. 3.6 Same as Fig. 3.4, but now for the nine-site configurations of (3.91). The *left panels* are for $\epsilon = 0.25$. Note that the solution is stable for small ϵ, but the negative Krein sign of the imaginary eigenvalues leads to a complex web of oscillatory instabilities for $\epsilon > 0.054$

3.3.4.2 Discrete Vortices

We now turn to the examination of discrete vortex solutions of families (ii) (both symmetric and supersymmetric) and (iv) that were previously considered theoretically in this chapter. The relevant features will be presented in a unified way for these solutions in Figs. 3.7, 3.8, 3.9, 3.10, 3.11, and 3.12. The top left panel will, in each case, show the profile of the vortex solution for a specific value of ϵ by means of contour plots of the real (top left), imaginary (top right), modulus (bottom left), and phase (bottom right) two-dimensional profiles. The right panels will in each case show the spectral plane of the linearization eigenvalues for the corresponding value of ϵ. The bottom panel shows the dependence of small eigenvalues as a function of ϵ, obtained via continuation methods from the AC limit of $\epsilon = 0$. In these graphs,

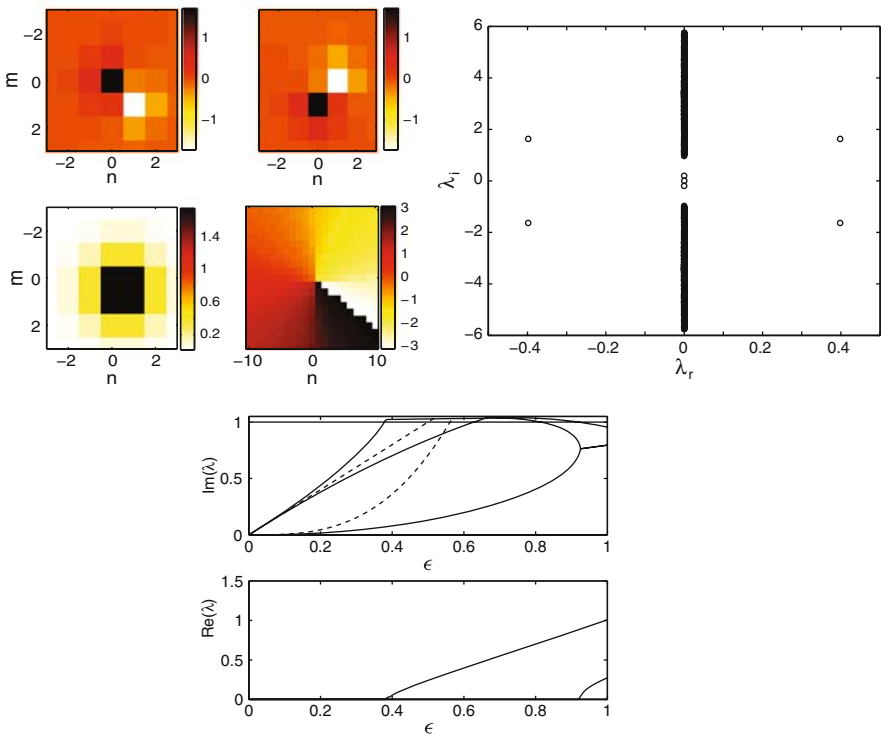

Fig. 3.7 The (supersymmetric) vortex cell with $L = M = 1$. The *top left panel* shows the profile of the solution for $\epsilon = 0.6$. The *subplots* show the real (*top left*), imaginary (*top right*), modulus (*bottom left*) and phase (*bottom right*) fields. The *top right panel* shows the spectral plane (λ_r, λ_i) of the linear eigenvalue problem (3.57). The *bottom panel* shows the small eigenvalues versus ϵ (the *top subplot* shows the imaginary part, while the *bottom* shows the real part). The *solid lines* show the numerical results, while the *dashed lines* show the results of the Lyapunov–Schmidt reductions. Reprinted from [14] with permission

as before, the solid lines will denote theoretical results, while the dashed ones, the result of the first-, second-, and higher order reductions presented above.

Figure 3.7 concerns the case of the supersymmetric vortex of charge $L = 1$ on the contour S_M with $M = 1$. In the second- and sixth-order reductions, the stability spectrum of the vortex solution has a pair of imaginary eigenvalues $\lambda \approx \pm i\sqrt{32}\epsilon^3$ and two pairs of imaginary eigenvalues $\lambda \approx \pm 2\epsilon i$. The latter pairs split along the imaginary axis beyond the second-order reductions. The larger pair of negative Krein signature becomes subject to a Hamiltonian–Hopf bifurcation for larger values of $\epsilon \approx 0.38$ upon collision with the continuous spectrum. The smaller pair of positive Krein signature disappears in the continuous spectrum for $\epsilon > 0.66$. The smallest pair of imaginary eigenvalues has negative Krein signature and a Hamiltonian–Hopf bifurcation occurs in the case for $\epsilon \approx 0.92$ due to collision with another pair of positive Krein signature bifurcating from the continuous spectrum.

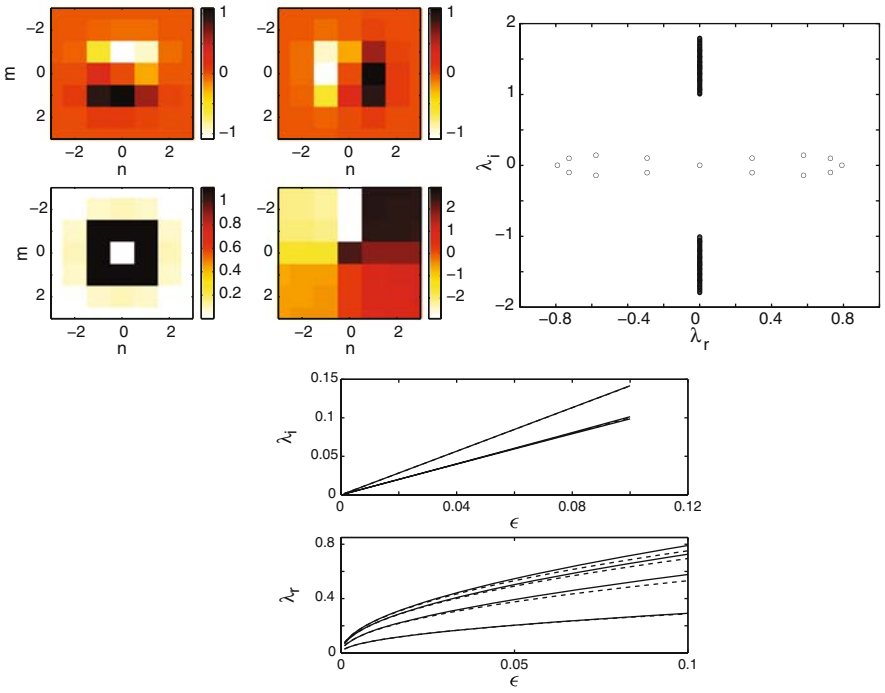

Fig. 3.8 The symmetric vortex with $L = 1$ and $M = 2$ for $\epsilon = 0.1$. Reprinted from [14] with permission

Figure 3.8 presents results for the symmetric vortex of charge $L = 1$ on the contour S_M with $M = 2$. There are three double and one simple real unstable eigenvalues in the first-order reductions, but all double eigenvalues split into the complex plane in the second-order reductions. The asymptotic result of Eq. (3.76) for eigenvalues $\lambda \approx \sqrt{\epsilon}\lambda_1 + \epsilon\lambda_2$ with $N = 8$, $a = \cos(\pi/4)$ and $b = \sin(\pi/4)$ is shown on Fig. 3.8 in very good agreement with numerical results.

Figure 3.9 shows results for the supersymmetric vortex with $L = M = 2$. The non-zero eigenvalues of the second- and sixth-order reductions consist of a pair of simple real eigenvalues $\lambda \approx \pm\epsilon\sqrt{\sqrt{80} - 8}$, a pair of simple imaginary eigenvalues $\lambda \approx \pm i\epsilon\sqrt{\sqrt{80} + 8}$, a pair of simple imaginary eigenvalues $\lambda \approx \pm 4i\epsilon^3$, and a pair of imaginary eigenvalues of algebraic multiplicity four at $\lambda \approx \pm i\epsilon\sqrt{2}$. The bottom right panel of Fig. 3.9 shows the splitting of multiple imaginary eigenvalues beyond the second-order reductions along the imaginary axis and also four subsequent oscillatory instabilities for larger values of ϵ ($\epsilon \approx 0.23, 0.5, 0.5,$ and 1.45). The other two pairs of purely imaginary eigenvalues collide with the band edge of the continuous spectrum at $\epsilon \approx 1.315$ and 1.395 and disappear into the continuous spectrum. Note, once again, the level of accuracy of our theoretical predictions in comparison with the direct numerical results, especially for the cases of small ϵ illustrated at the bottom left panel of Fig. 3.9. We will return to this structure below,

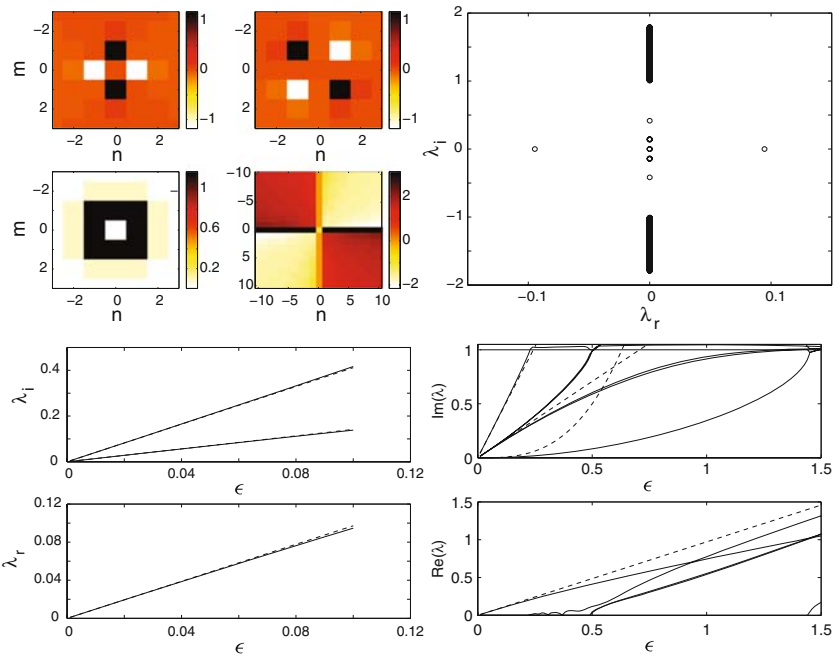

Fig. 3.9 The supersymmetric vortex with $L = M = 2$ for $\epsilon = 0.1$. The *bottom right panel* is an extension of the *bottom left panel* to larger values of ϵ. Reprinted from [14] with permission

using it as a case example of the "mathematical intuition" that our reductions offer on the origin of the observed dynamical instability and how this can be avoided in such a case.

Figure 3.10 shows results for the symmetric vortex with $L = 3$ and $M = 2$. The first-order reductions predict three pairs of double imaginary eigenvalues, a pair of simple imaginary eigenvalues and a double zero eigenvalue. The double eigenvalues split in the second-order reductions along the imaginary axis, given by (3.76) with $N = 8$, $a = \cos(3\pi/4)$ and $b = \sin(3\pi/4)$. The seven pairs of imaginary eigenvalues lead to a cascade of seven complex quartets of eigenvalues emerging for larger values of ϵ due to their collisions with the continuous spectrum. The first bifurcation when the symmetric vortex becomes unstable occurs for $\epsilon \approx 0.096$. It is interesting to note in connection to this solution the sharp contrast between this result (i.e., the fact that a solution with $L = 3$ may be *stable*, while the lower charge $L = 2$ solution is *always unstable* over the same contour) and the continuum NLS intuition; see, e.g., [22] for relevant analytical considerations and [23, 24] for numerical results. The latter indicates that over this discrete contour higher charge vortices are more prone to instability than the lower charge ones. On the contrary, the stability of the discrete $L = 3$ structure was first observed in [25].

Zero parameter asymmetric vortices of family (iv) on the contour S_M with $M = 2$ are shown in Fig. 3.11 for $L = 1$ and in Fig. 3.12 for $L = 3$. In the case of Fig. 3.11, all the phase differences between adjacent sites in the contour are $\pi/6$, except for

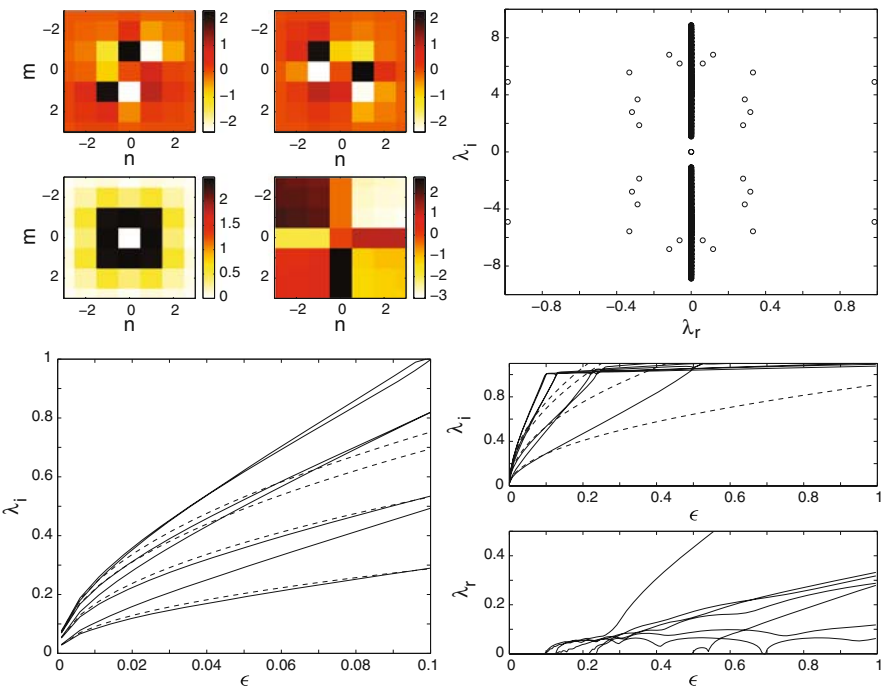

Fig. 3.10 The symmetric vortex with $L = 3$ and $M = 2$ for $\epsilon = 1$. Reprinted from [14] with permission

the last one which is $5\pi/6$, completing a phase trip of 2π for a vortex of topological charge $L = 1$. Eigenvalues of the matrix $\mathcal{M}_1$ in the first-order reductions can be computed numerically as follows: $\mu_1^{(1)} = -1.154$, $\mu_2^{(1)} = 0$, $\mu_3^{(1)} = 0.507$, $\mu_4^{(1)} = 0.784$, $\mu_5^{(1)} = 1.732$, $\mu_6^{(1)} = 2.252$, $\mu_7^{(1)} = 2.957$, and $\mu_8^{(1)} = 3.314$. As a result, the corresponding eigenvalues $\lambda \approx \pm\sqrt{2\mu^{(1)}\epsilon}$ yield one pair of imaginary eigenvalues and six pairs of real eigenvalues, in agreement with our numerical results. The bottom panel of Fig. 3.11 shows that two pairs of real eigenvalues collide for $\epsilon \approx 0.047$ and 0.057 and lead to two quartets of eigenvalues.

In the case of Fig. 3.12, all the phase differences in the contour are $5\pi/6$, except for the last one which is $\pi/6$, resulting in a vortex of topological charge $L = 3$. Eigenvalues of the matrix $\mathcal{M}_1$ are found numerically as follows: $\mu_1^{(1)} = -3.314$, $\mu_2^{(1)} = -2.957$, $\mu_3^{(1)} = -2.252$, $\mu_4^{(1)} = -1.732$, $\mu_5^{(1)} = -0.784$, $\mu_6^{(1)} = -0.507$, $\mu_7^{(1)} = 0$, and $\mu_8^{(1)} = 1.154$. Consequently, this solution has six pairs of imaginary eigenvalues and one pair of real eigenvalues. The first Hamiltonian–Hopf bifurcation in this case occurs for $\epsilon \approx 0.086$.

It is interesting to note in passing that this approach is equally well-suited to address not just "isotropic" square lattices, where the x and y directions are equivalent, but also even *anisotropic* such lattices, where for instance the coefficient of the discrete Laplacian has a different prefactor (e.g., ϵ and $\epsilon\alpha$, respectively) in the two

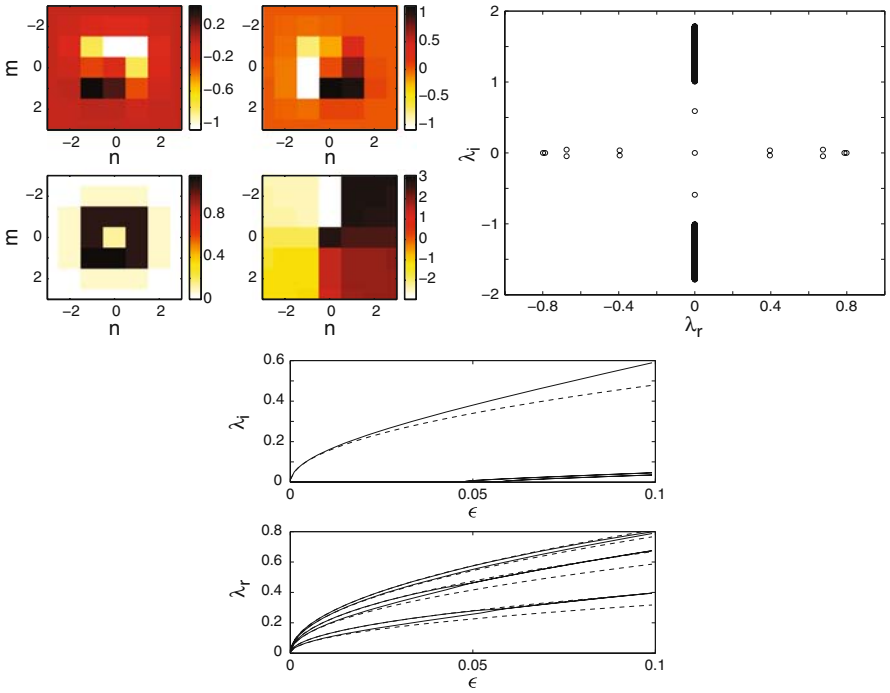

Fig. 3.11 The asymmetric vortex with $L = 1$ and $M = 2$ for $\epsilon = 0.1$. Reprinted from [14] with permission

different directions. Although, we won't analyze this possibility in more detail here, the relevant details can be found by the interested reader in the work of [26].

3.3.4.3 Stabilization of Unstable Waves

One of the most remarkable features of the above developed technology for the detection of the coherent structures and their linear stability in dynamical lattices of the DNLS type is its "mathematical intuition" about the nature of the encountered instabilities and how to potentially eliminate them.

As a case example of this type, we consider one of the most prototypical unstable vortex configurations considered above, namely the vortex with $L = M = 2$. The examination of the real eigenmode leading to the direct instability of the $S = 2$ vortex (that has support over the central site that we denote by a double zero subscript in what follows), as well as the apparent mediation of the instability by means of the central site (see below), lead us to consider the possibility of having an "impurity" at the central site, e.g., a strong localized potential such as a laser beam in BECs or an inhomogeneity in a photorefractive crystal, enforcing $\phi_{0,0} = 0$. More specifically, what we observe mathematically is that the additional terms in the second order reductions that appear to mediate the instability are the terms in the corresponding

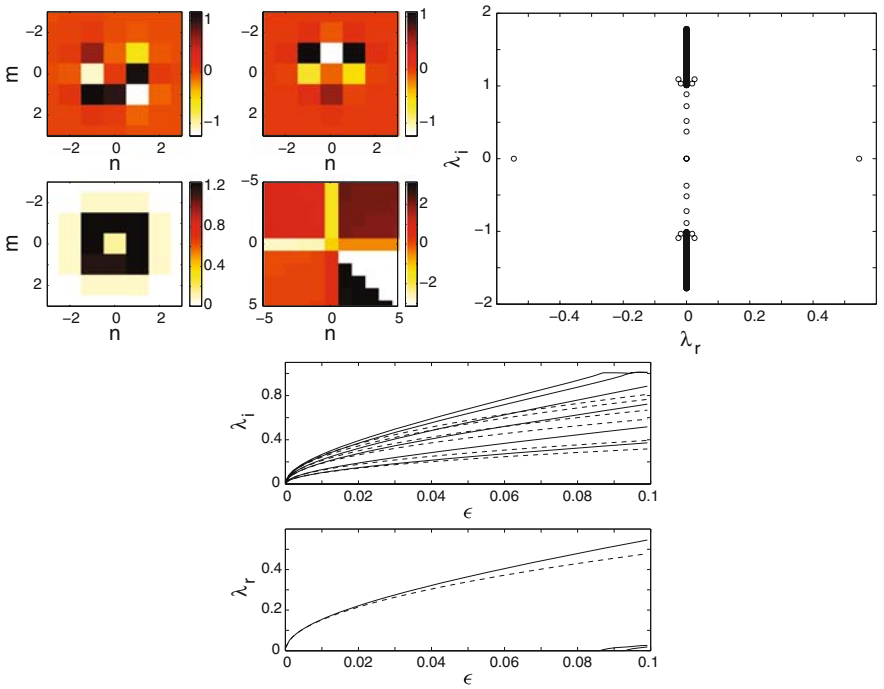

Fig. 3.12 The asymmetric vortex with $L = 3$ and $M = 2$ for $\epsilon = 0.1$. Reprinted from [14] with permission

reduction matrix $\mathcal{M}_2$ coupling the sites adjacent to $(0, 0)$. If we therefore eliminate this central site, disallowing the "communication" between its neighboring sites, then the bifurcation function g_j^2 of the form

$$g_j^2 = \frac{1}{2}\sin(\theta_{j+1} - \theta_j)\left[\cos(\theta_j - \theta_{j+1}) + \cos(\theta_{j+2} - \theta_{j+1})\right]$$
$$+\frac{1}{2}\sin(\theta_{j-1} - \theta_j)\left[\cos(\theta_j - \theta_{j-1}) + \cos(\theta_{j-2} - \theta_{j-1})\right]$$
$$+\left[\sin(\theta_j - \theta_{j+2}) + \sin(\theta_j - \theta_{j+4}) + \sin(\theta_j - \theta_{j-2})\right](\delta_{j,2} + \delta_{j,4} + \delta_{j,6} + \delta_{j,8})$$

(with $1 \leq j \leq 8$ and where δ denotes the Kronecker symbol) lacks the last term, since these are interactions "mediated" by the now inert site. The second-order Jacobian is then much simpler and acquires the form $(\mathcal{M}_2)_{j,k} = 1$ for $j = k$, $-1/2$ for $j = k \pm 2$, and 0 for $|j - k| \neq 0, 2$. One can then repeat the calculation of the corresponding eigenvalues, via the discrete Fourier transform, to obtain the characteristic equation

$$\left(\lambda_1 + 2i\sin(\frac{j\pi}{4})\right)^2 = 0, \qquad j = 1, \ldots, 8. \tag{3.92}$$

This results into three eigenvalues of algebraic multiplicity four, namely $\lambda = 0$ and $\lambda = \pm\epsilon i\sqrt{2}/2$. There are also two double eigenvalues $\lambda = \pm 2\epsilon i$. The crucial observation, however, is that in this case, there are no real eigenvalues immediately present as $\epsilon \neq 0$ and hence the discrete vortex with $S = 2$ will be *linearly stable*, due to the stabilizing effect of the impurity (or, to be more precise, due to the absence of the instability mediated by the central site).

The stabilization of the relevant structure is clearly shown in Fig. 3.13. The figure illustrates the principal relevant eigenvalues in the case of the inert central site in the left panels, clearly demonstrating not only the validity of the theoretical reduction results presented above, but most importantly the absence of any eigenvalues with non-zero real part for small ϵ. Note that the instability only sets in due to a complex quartet in this case for $\epsilon > 0.36$, which indicates that under the present conditions the stability range of the vortex of $L = 2$ is comparable to that of $L = 1$ (which is stable for $\epsilon < 0.38$). As a result, the right panel shows that for $\epsilon = 0.2$, the same structure with the same perturbation that would have clear instability dynamics for the uniform chain, would no longer be subject to such an instability in the chain with the inert central defect site. These results were first presented in [27].

Interestingly, this suggestion has motivated further studies on this topic such as the work of [28], which suggested on a purely numerical basis the consideration of a cross-like vortex of $L = 2$, such as the one illustrated in the left panels of Fig. 3.14. Note that in this case, once again "reduced communication" is achieved between the four sites previously cross-talking through the central node of the contour; however, instead of this being realized through the central site being inert, here, it is achieved geometrically through increasing the distance between these sites (in the

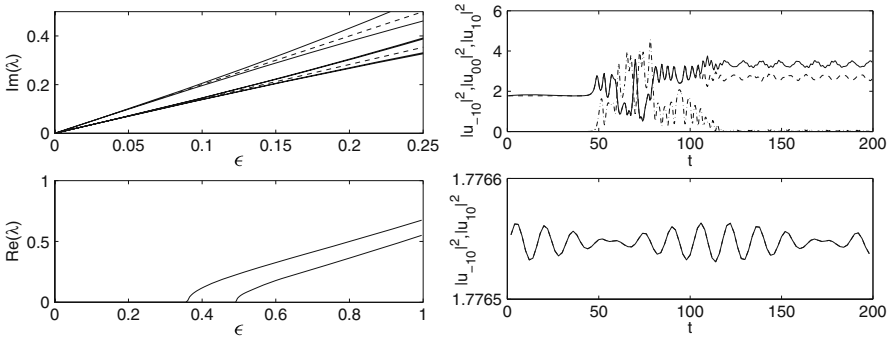

Fig. 3.13 From [27]: the *left panels* of the figure show the imaginary (*top panels*) and real (*bottom panels*) parts of the eigenvalues initially at the origin of the spectral plane for the vortex with $L = M = 2$, but with the central site inert. We can see that, contrary to the case where the central site is present, the structure is linearly stable for small ϵ; note again the agreement between the theoretical prediction of the reductions (*dashed line*) and the full numerics (*solid line*). This results in a dynamical evolution shown in the *right panels* for $\epsilon = 0.2$, where some of the main sites of the configuration are shown in the presence (*top panels*) or absence (*bottom panels*) of the central site. Note how the same configuration which is unstable in the *top* (for the same initial perturbation) becomes stabilized in the *bottom*

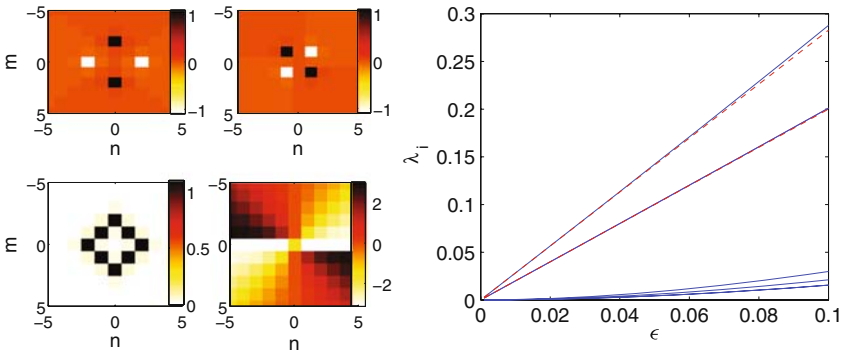

Fig. 3.14 The *left panels* show a typical example of the vortex cross of $L = 2$ which is stable for small ϵ according to the *right panel* illustrating the relevant eigenvalues close to $\lambda = 0$ (which are all imaginary). Note once again the agreement between the result of the analytical reductions (*dashed lines*) and the numerical findings (*solid lines*)

resulting rhombic pattern). In fact, we have studied this structure at the level of the analytical reductions, finding from the relevant Jacobian of the bifurcation equations that it should have a single eigenvalue pair $\lambda = \pm\sqrt{8}\epsilon i$, a double eigenvalue pair $\lambda = \pm 2\epsilon i$, as well as four pairs of eigenvalues of a higher order (not discussed in detail here) which are also imaginary (see the right panel of Fig. 3.14). The relevant theoretical predictions are compared to full numerical results for small ϵ in Fig. 3.14, illustrating, once again, the usefulness of the method in providing quantitative information about the stability (as well as the stabilization) of the various configurations.

3.3.4.4 Solitons and Vortices in Non-Square Lattices

The considerations presented above in the case of square lattices can be straightforwardly generalized to different types of lattices (such as hexagonal or honeycomb ones), where the number of nearest neighbors is different (six and three, respectively) and hence we expect quantitative, and perhaps even qualitative changes in the relevant phenomenology. As a concrete example of this type, we will consider for definiteness the DNLS in a hexagonal geometry

$$i\frac{du_{m,n}}{dz} = -\epsilon\left(\sum_{<m',n'>} u_{m',n'} - 6u_{m,n}\right) - |u_{m,n}|^2 u_{m,n}, \tag{3.93}$$

where the summation is meant over the six nearest neighbors (denoted by $\langle m', n'\rangle$) of the site (m, n). This type of setting was originally considered in [29], while subsequent works such as [30] extended it also to Klein–Gordon lattices and the examination of breather states therein.

In this context, selecting a simple hexagonal contour with a central inert site, it is straightforward to construct a configuration with topological charge S over the contour, provided that we select the AC limit solutions in the form $u_j = \exp(i\theta_j)\exp(it)$

(normalizing, without loss of generality, the propagation constant to unity), where $\theta_j = 2\pi jS/6$ and $j = 1, \ldots, 6$ for the six sites constituting the relevant contour. It is straightforward to see that this configuration yields non-trivial phase profiles for $S = 1$ and 2, while for $S = 3$ it yields a "discrete hexapole" (i.e., not a genuine $S = 3$ vortex structure, but instead a real configuration emulating that waveform in the discrete setting), which can nonetheless also be considered within the analytical framework provided below; also $S = 0$ corresponds to the case of an in-phase structure, that we should expect to be unstable. It should also be noted that this framework works not only for contours of "size" $N = 6$ as will be considered here, but also for ones with $N = 3$ (in that case, e.g., the $\theta_j = 2\pi jS/N$ with $N = 3$), as in [30]. A brief discussion of the results in that context is given below. The results below follow closely the presentation of [31].

We can straightforwardly adapt the calculations presented above to formulate the persistence conditions for the configuration in the presence of finite coupling as:

$$g_j \equiv \sin(\theta_j - \theta_{j+1}) + \sin(\theta_j - \theta_{j-1}) = 0 \tag{3.94}$$

for all $j = 1, \ldots, 6$. Then one can also adapt the stability conditions obtained previously based on the *Jacobian* $\mathcal{M}_{jk} = \partial g_j/\partial\theta_k$ and its eigenvalues γ_j in connection to the eigenvalues of the full linearization $\lambda_j = \sqrt{2\gamma_j\epsilon}$ (to leading order). In the present setting, the Jacobian matrix is given by the expression of (3.35), where the factor $a \equiv \cos(\theta_{j+1} - \theta_j) = \cos(\pi S/3)$ appears in all the elements of the matrix (multiplied by 2 for the diagonal elements and by -1 for the off-diagonal ones). As a result, the eigenvalue problem for the γ's is equivalent to

$$a(2x_n - x_{n+1} - x_{n-1}) = \gamma x_n, \tag{3.95}$$

which can be solved by discrete Fourier transform (i.e., using for the eigenvector $x_n \sim \exp(i\pi jn/3)$), yielding $\gamma_j = 4a\sin^2(\pi j/6)$ and hence, finally,

$$\lambda_j = \pm\sqrt{8\epsilon\cos\left(\frac{\pi S}{3}\right)\sin^2\left(\frac{\pi j}{6}\right)}. \tag{3.96}$$

More specifically, in the case of $S = 1$ this predicts that the fundamental vortex solution will be *unstable* due to two double real eigenvalue pairs with $\lambda = \pm\sqrt{\epsilon}$ and $\lambda = \pm\sqrt{3\epsilon}$ and a single real eigenvalue pair of $\lambda = \pm 2\sqrt{\epsilon}$ (one of the six eigenvalues of the Jacobian is zero due to the phase invariance of the equation), while on the other hand, the $S = 2$ configuration will be *stable* because its eigenvalues will be those of $S = 1$ multiplied by the complex unity (and hence will be all imaginary). It is interesting to note in passing that for $S = 0$ and 3 the above theoretical prediction encompasses the instability and stability, respectively, of a hexagonal discrete soliton with in-phase and out-of-phase nearest-neighbor excitations.

Note that these results can be straightforwardly extended to the three-site contour of the hexagonal lattice, in which case $N = 3$, and therefore the corresponding

expression will become

$$\lambda_j = \pm\sqrt{8\epsilon\cos\left(\frac{2\pi S}{3}\right)\sin^2\left(\frac{\pi j}{3}\right)}. \tag{3.97}$$

It is also interesting to point out that the results would not change to this leading order for a six-site contour of a honeycomb lattice, since the (absent in that case) inert central site of the hexagonal contour is not accounted for in the above leading order calculation. Finally, it should be pointed out that the stability conclusions obtained above should be expected to be reversed for $\epsilon < 0$ (the defocusing case that we will examine in more detail in Chap. 5). In particular, the in-phase solution will be stable, while the out-of-phase hexapole will be unstable, and similarly the charge $S = 1$ vortex will be the stable one, while the $S = 2$ vortex will be unstable.

We test these predictions in a prototypical case, namely for the $S = 1$ and 2 vortices in the six-site hexagonal lattice contour in Fig. 3.15. The four left panels of the figure represent a typical example of an $S = 1$ vortex (for $\epsilon = 0.025$, close to the AC limit). The second row illustrates the eigenvalues of the associated linearization of Eq. (3.93) around the vortex solution, revealing the presence of five unstable eigenmodes (with non-zero real parts), in agreement with the theoretical prediction. Interestingly, the double eigenvalues of the above theoretical prediction split into complex quartets (a similar feature was observed in the case of $S = 1$ vortices on eight-site square contours earlier in this chapter). Note the quality of the comparison of the theoretical prediction of the modes' growth rates with respect to the corresponding numerical results for small ϵ. The right four panels of Fig. 3.15 represent the case of $S = 2$ which, again in accordance with our theoretical prediction, is indeed found to be linearly stable for small coupling (no eigenvalues with non-zero real part). While in that case the double eigenvalues split, they still follow fairly accurately the trends of the relevant theoretical predictions. These results illustrate

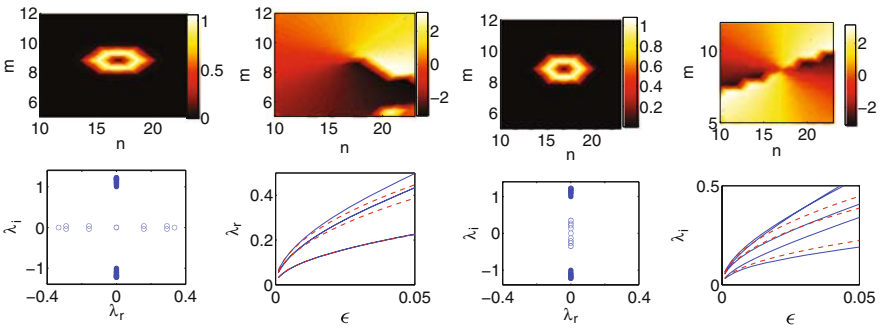

Fig. 3.15 Amplitude and phase of the $S = 1$ vortex (*left panels*) and $S = 2$ vortex (*right panels*), for $\epsilon = 0.025$. The corresponding spectral planes (λ_r, λ_i) of the linearization eigenvalues $\lambda = \lambda_r + i\lambda_i$ are shown in the corresponding *bottom left panels*. The respective *bottom right panels* show the eigenvalues bifurcating from the spectral plane origin as numerically obtained (*solid*) and theoretically predicted from Eq. (3.96) (*dashed*)

that the techniques presented in this chapter are by no means restricted to square lattices, but rather can be directly adapted to address more general lattices, as well as potentially DNLS equations on graphs with different types of connectivities.

References

1. Sulem, C., Sulem, P.L.: The Nonlinear Schrödinger Equation. Springer-Verlag, New York (1999) 56
2. Chiao, R.Y., Garmire, E., Townes, C.H.: Phys. Rev. Lett. **13**, 479 (1964) 56, 58
3. Flach, S., Kladko, K., MacKay, R.S.: Phys. Rev. Lett. **78**, 1207 (1997)
4. Weinstein, M.I.: Nonlinearity **12**, 673 (1999)
5. Kastner, M.: Phys. Rev. Lett. **93**, 150601 (2004)
6. Grillakis, M.: Commun. Pure Appl. Math. **43**, 299 (1990) 58
7. Grillakis, M.: Commun. Pure Appl. Math. **41**, 745 (1988) 58
8. Grillakis, M., Shatah, J., Strauss, W.: J. Func. Anal. **94**, 308 (1990) 58
9. Kapitula, T., Kevrekidis, P.G., Sandstede, B.: Physica D **195**, 263 (2004) 58
10. Kapitula, T., Kevrekidis, P.G., Sandstede, B.: Physica D **201**, 199 (2005) 58
11. Kevrekidis, P.G., Rasmussen, K.Ø., Bishop, A.R.: Phys. Rev. E **61**, 2006 (2000) 57
12. Vakhitov, M.G., Kolokolov, A.A.: Radiophys. Quantum Electron. **16**, 783 (1973) 57, 58
13. Fibich, G., Gaeta, A.L.: Opt. Lett. **25**, 335 (2000) 57, 58
14. Pelinovsky, D.E., Kevrekidis, P.G., Frantzeskakis, D.J.: Physica D **212**, 20 (2005) 58, 60, 67, 76, 88, 89, 90
15. Malomed, B.A., Kevrekidis, P.G.: Phys. Rev. E **64**, 026601 (2001)
16. Yang, J., Musslimani, Z.: Opt. Lett. **28** 2094–2096, (2003) 61
17. MacKay, R.S., Aubry, S.: Nonlinearity **7**, 1623 (1994) 61
18. Chow, S.N., Hale, J.K.: Methods of Bifurcation Theory. Springer-Verlag, Heidelberg (1982) 61
19. Golubitsky, M., Schaeffer, D.G.: Singularities and Groups in Bifurcation Theory. vol. 1, Springer-Verlag, New York (1985) 61, 62, 63
20. Kapitula, T., Kevrekidis, P.G., J. Phys. A **37**, 7509 (2004) 64, 66
21. Alexander, T.J., Sukhorukov, A.A., Kivshar, Yu.S.: Phys. Rev. Lett. **93**, 063901 (2004) 64
22. Pego, R.L., Warchall, H.: J. Nonlin. Sci. **12**, 347 (2002) 90
23. Carr, L.D., Clark, C.W.: Phys. Rev. A **74**, 043613 (2006) 90
24. Herring, G., Carr, L.D., Carretero-González, R., Kevrekidis, P.G., Frantzeskakis, D.J.: Phys. Rev. A **77**, 023625 (2008) 90
25. Kevrekidis, P.G., Malomed, B.A., Zhigang, C., Frantzeskakis, D.J.: Phys. Rev. E **70**, 056612 (2004) 90
26. Kevrekidis, P.G., Frantzeskakis, D.J., Carretero-González, R., Malomed, B.A., Bishop, A.R.: Phys. Rev. E **72**, 046613 (2005) 92
27. Kevrekidis, P.G., Frantzeskakis, D.J.: Phys. Rev. E **72**, 016606 (2005) 94
28. Öster, M., Johansson, M.: Phys. Rev. E **73**, 066608 (2006) 94
29. Kevrekidis, P.G., Malomed, B.A., Gaididei, Yu.B.: Phys. Rev. E **66**, 016609 (2002) 61, 95
30. Koukouloyannis, V., MacKay, R.S.: J. Phys. A: Math. Gen. **38**, 1021–1030 (2005) 95, 96
31. Law, K.J.H., Kevrekidis, P.G., Koukouloyannis, V., Kourakis, I., Frantzeskakis, D.J., Bishop, A.R.: Phys. Rev. E **78**, 066610 (2008) 96